atmosphere

MDPI

Article

Analysis of the Post-Cyclonic Physical Flood Susceptibility and Changes of Mangrove Forest Area Using Multi-Criteria Decision-Making Process and Geospatial Analysis in Indian Sundarbans

Biraj Kanti Mondal [1,*], Sanjib Mahata [1], Tanmoy Basu [2], Rima Das [3], Rajib Patra [4], Kamal Abdelrahman [5], Mohammed S. Fnais [5] and Sarbeswar Praharaj [6]

[1] Department of Geography, Netaji Subhas Open University, Kolkata 700064, India; sanjibmahata5@gmail.com
[2] Department of Geography, Katwa College, Purba Bardhaman 713130, India; tanmoybasu.2017@gmail.com
[3] Department of Geography, Bhangar Mahavidyalaya, South 24 Parganas 743502, India; mampirimadas@gmail.com
[4] Department of Geography, Ramsaday College, Howrah 711401, India; rpgeo22@gmail.com
[5] Department of Geology and Geophysics, College of Science, King Saud University, Riyadh 11451, Saudi Arabia; khassanein@ksu.edu.sa (K.A.); mfnais@ksu.edu.sa (M.S.F.)
[6] Knowledge Exchange for Resilience, School of Geographical Sciences and Urban Planning, Arizona State University, Tempe, AZ 85281, USA; s.praharaj@asu.edu
* Correspondence: birajmondal.kolkata@gmail.com; Tel.: +91-8240506428

Abstract: Tropical cyclones, one of the most extreme and destructive meteorological incidents, cause extensive damage to lives and livelihoods worldwide. This study utilized remotely sensed data along with multi-criteria decision-making, geospatial techniques, and major cyclonic events *Aila*, *Amphan*, and *Yaas* to identify the changes in the vulnerability of cyclone-induced floods in the 19 community development blocks of Indian Sundarbans in the years 2009–2010, 2020–2021, and 2021–2022 (the post-cyclonic timespan). The Sundarbans are a distinctive bioclimatic region located in a characteristic geographical setting along the West Bengal and Bangladesh coasts. In this area, several cyclonic storms had an impact between 2009 and 2022. Using the variables NDVI, MNDWI, NDMI, NDBI, BSI, and NDTI, Landsat 8 Operational Land Imager, Thermal Infrared Sensor, Resourcesat LISS-III, and AWiFS data were primarily utilized to map the cyclonic flood-effective zones in the research area. The findings indicated that the coastline, which was most impacted by tropical storms, has significant physical susceptibility to floods, as determined by the AHP-weighted overlay analysis. Significant positive relationships ($p < 0.05$, $n = 19$ administrative units) were observed between mangrove damage, NDFI, and physical flood susceptibility indicators. Mangrove damage increased with an increase in the flood index, and vice versa. To mitigate the consequences and impacts of the vulnerability of cyclonic events, subsequent flood occurrences, and mangrove damage in the Sundarbans, a ground-level implementation of disaster management plans proposed by the associated state government, integrated measures of cyclone forecasting, mangrove plantation, coastal conservation, flood preparedness, mitigation, and management by the Sundarban Development Board are appreciably recommended.

Keywords: tropical cyclone; flood susceptibility; AHP; weighted overlay; NDFI; Sundarbans

check for updates

Citation: Mondal, B.K.; Mahata, S.; Basu, T.; Das, R.; Patra, R.; Abdelrahman, K.; Fnais, M.S.; Praharaj, S. Analysis of the Post-Cyclonic Physical Flood Susceptibility and Changes of Mangrove Forest Area Using Multi-Criteria Decision-Making Process and Geospatial Analysis in Indian Sundarbans. *Atmosphere* **2024**, *15*, 432. https://doi.org/10.3390/atmos15040432

Academic Editors: Yubin Li and Jimy Dudhia

Received: 11 January 2024
Revised: 26 February 2024
Accepted: 27 March 2024
Published: 30 March 2024

Copyright: © 2024 by the authors. Licensee MDPI, Basel, Switzerland. This article is an open access article distributed under the terms and conditions of the Creative Commons Attribution (CC BY) license (https://creativecommons.org/licenses/by/4.0/).

1. Introduction

Mangrove forests act as shock absorbers in the Sundarbans region; they protect against tides and waves [1] and persist with ecological revitalization [2]. In this region, climatic hazard affects riverbank erosion, and it has a wide impact on the loss of the Sundarbans mangrove forest (SMF) [3]. The Sundarbans, a region recognized by UNESCO as a world heritage site because of its rich biodiversity, were severely damaged and destroyed by

the super cyclones [4]. It was revealed from a recent study that, from 1986 to 2012, about 124.418 square km and, in 2020, 136.77 square km of mangrove forest cover was lost in the Sundarbans [5]. Furthermore, climatic hazards resulting from global climate change affect sea level rise, and it is rising faster than ever before (2.6–4 mm/year) [6]. There are many consequences of this, such as the erosion of riverbanks, the loss of the Sundarbans mangrove forests, deforestation, coastal erosion, coastal floods, the inundation of saline water into fields, and an increase in the number of tidal creeks. Several tropical cyclones, including *Aila* (2009), *Bulbul* (2019), *Amphan* (2020), and *Yaas* (2021), hit the region, resulting in flood conditions. These fierce cyclones battered the mangrove forest of the Sundarbans, destroying several mangrove forests and ravaging local villages. Most of these cyclones damaged and collapsed embankments, inundating several islands. Due to the cyclonic flood, the victims lost their homesteads and croplands, as well as their survival strategy in the riverbank areas. Moreover, farmers and many other people are largely affected by storm surges and flood inundation, as they lose their source of income and their habitat. Tropical cyclones (TCs) are one of the most destructive natural phenomena worldwide. This extreme meteorological incident causes extensive damage to lives and livelihoods. The seasonal and year-wise variabilities of TCs all across the globe have been the foremost-focused areas over the past few decades. Models and observations are usually compared in detection and attribution studies to investigate the reasons behind observed climate changes or occurrences. To control the effects of many environmental factors on the ground, the use of remote sensing and spatial analysis has substantially increased. The supportive discussion regarding the statement is followed in the studies [7–10]. Super cyclone *Amphan*, one of the strongest tropical cyclones ever recorded, had its origins in the Bay of Bengal, and related research [4] examined the effects of the *Amphan* Disaster on the Sundarbans. The influence zone is the region that the Sundarbans' existence affects because of storm surge flooding. The inundation area and depth are two important factors that determine impact zones in both scenarios [11].

1.1. Studies on the Impact of Tropical Cyclones and Flood Occurrences in Sundarbans

Regarding the cyclonic storm and associated flood vulnerability, previous research was reviewed in this study. The Sundarbans mangrove forest is crucial to the protest against coastal flooding. Due to the high tidal amplitude and complicated coastline geometry, there is a high level of risk for the coastal areas of West Bengal, Bangladesh, and Myanmar in *Aila* (2009) [12]. The increasing frequency and severity of climate change-induced extreme events increase the pressure on forest ecosystem services, potentially leading to extinction [13]. The recent tropical cyclone *Aila* caused incremental stresses on socio-economic conditions, forcing people to change their livelihoods to forest resources [13]. The research [14] examined how vulnerable people now face uncertainty following the landfall of super cyclone *Amphan* in the Sundarbans region. To evaluate the harm caused by cyclone *Amphan*, this study created a remote sensing-based methodology that combined satellite data from optical, radar, and LiDAR platforms [15]. A total of 6821 square km of land was inundated even 10 days after the cyclone, and there was a 0.2-unit decline in NDVI in 3.45 square km of Sundarbans mangrove forest [15]. The possible impacts of storm surge flooding on the Sundarbans mangrove ecosystem were evaluated by the study [16]. Furthermore, the continuous loss of this important ecosystem might have a severe impact on future cyclone-related dangers in Bangladesh's Sundarbans region [16]. Due to poverty and cyclones, Odisha is extremely vulnerable to climate variability and change. The Kendrapada district in Odisha was the subject of a case study to lessen vulnerability and increase resilience [17]. Over the past 250 years, mangrove cover has altered as a result of human involvement, upstream development, catastrophic weather occurrences, and climate change [18]. This study looked at changes between 2000 and 2020 in mangrove extent, genus mix, and health indices [19]. Mangroves' size and health have declined, which puts the Indian Sundarbans in long-term danger of extinction, especially in the case of climate change and sea level rise.

1.2. Review of the Geospatial Analysis on the Cyclonic Flood Assessment in Sundarbans

The monitoring of mangrove forest dynamics in the Sundarbans in Bangladesh and India using multi-temporal satellite data from 1973 to 2000 was conducted in [20]. An integrated vulnerability assessment framework and one of the most popular methods for estimating flood vulnerability are statistical methods and weighting allocation [21]. Time series of satellite images, socioeconomic census data, focus group discussion, and other techniques have been utilized to assess the effects of recent tropical storms on the ecosystem of the Sundarbans mangrove forest in Bangladesh and India [22]. Studies have also used multi-temporal satellite data and geographic information system features to identify the flood susceptibility zones in the Bongaon sub-division of North 24 Parganas [23]. The efficacy of support vector machine (SVM) models, modified frequency ratio models, and conventional frequency ratio models have been maneuvered in the analysis of storm surge and flood susceptibility [24]. A recent study [25] contrived a composite vulnerability index to evaluate the vulnerability of villages in India's Sundarbans Biosphere Reserve (SBR) to storm surge floods. The categorization of 19 Sundarbans blocks into very high, high, moderate, and low vulnerability areas using a cyclone disaster vulnerability index was proposed in [26]. The results of that study found that non-coastal blocks have a higher vulnerability score in comparison to other coastal blocks [26]. The research [27] suggested an integrated geostatistical and geoinformatics-based strategy. Results of the investigation showed that 19.5% of mouzas and 15.33% of the population in the southern portion of the island are at high risk [27]. The coastal vulnerability index (CVI) assisted in the assessment of physical and coastal vulnerability conditions and helped identify islands that need immediate attention to lessen the impact of hazards caused by climate change [28]. In the Sundarbans region of India, a multi-criteria decision-making technique was used to evaluate the block-level risk of cyclones [29]. The results of the weighted analysis showed that proximity to the coast and distance from the cyclone tract had the highest vulnerability exposure, windspeed had the highest hazard score, and proximity to the cyclone shelter had the highest hazard score [29], and they also examined the fact that natural disasters like cyclones have a terrible impact on people's lives and way of life [29]. Therefore, designing adaptation strategies in major cyclone-prone areas requires a risk assessment in the Sundarbans.

1.3. Summary of the Literature Review and Research Gap

The prior research utilized analyses of cyclonic storms such as *Aila* and *Amphan*, which caused significant harm to the Sundarbans mangrove forest, to underscore the possibility of forest ecosystem services disappearing as a result of climate change. The loss of this important ecosystem may have a major effect on the region's future cyclone-related dangers. Utilizing multi-temporal satellite data from the 1990s, researchers have examined the effects of natural hazards in the Sundarbans mangrove forest located in the deltaic regions of India and Bangladesh. Furthermore, the coastal vulnerability index identifies areas that are vulnerable to cyclones, and designing adaptation measures in these areas depends heavily on risk assessment. The comparison of the spectral indices-based flood index with the flood susceptibility or vulnerability index in the Sundarbans region is one minor study gap in the earlier studies. There are likewise few noticeable correlations between the various flood risk indicators and the flood index. The lack of evidence supporting a connection between the flood index and the mangrove damage index derived from remote sensing is another problem. Last but not least, a scholarly brief about the Sundarbans region's block-level study about the forecast of current problems exists. The present study used a multi-criteria decision-making process and geospatial analysis to investigate the physical susceptibility of flood hazards in the Indian Sundarbans region. It also looked into the damage and alterations to mangroves in the Sundarbans between 2009 and 2022. The post-cyclonic flood risk zones (2010, 2021, and 2022, the targeted years of the present study for flood susceptibility analysis) and their predictions were identified using satellite imagery and geospatial algorithms. This study also used correlation-regression analysis

between NDFI and specific spectral indices of flood susceptibility to determine physical flood susceptibility probability zones in the blocks of the study area. This study attempted to answer specific research questions:

1. What are the major indicators of physical susceptibility to floods in the study area?
2. Which area is the most vulnerable and susceptible to flood occurrences in the C.D. blocks under the Indian Sundarbans?
3. What is the relationship between flood (NDFI) and mangrove damage, and what are the major indicators of physical susceptibility to flooding?

2. Materials and Methods

2.1. Study Area

The Sundarbans region, the present study area, is a unique bioclimatic zone in a typical geographical situation. In the region where Ganga, Brahmaputra, and Meghna meet the Bay of Bengal, many active deltas spread across the coasts of India and Bangladesh. Being the largest area of mangroves in the world, the Sundarbans hold an exceptional level of biodiversity. The Indian Sundarbans region (ISR), located on the north-east coast of India, is bounded between 21°3′ North and 22°40′ North latitude and 88°03′ East and 89°07′ East longitude. It covers an area of approximately 9630 square km, comprising nineteen blocks from North and South Twenty-Four Parganas [30]. The Sundarbans are comprised of a total of 6 C.D. blocks from the North Twenty-Four Parganas named Haroa, Minakhan, Sandeshkhali-I, Sandeshkhali-II, Hasnabad, and Hingalganj and 13 C.D. blocks from the South Twenty-Four Parganas named Canning-I, Canning-II, Mathurapur-I, Jaynagar-I, Jaynagar-II, Kultali, Basanti, Gosaba, Mathurapur-II, Kakdwip, Sagar, Namkhana, and Patharpratima (Figure 1). ISR, which is also the habitat of over 5 million people, is an ecologically fragile and climatically vulnerable region [31,32]. Since 2009, the Sundarbans have been battered by several tropical cyclones, such as *Aila* (May 2009), *Komen* (July 2015), *Fani* (May 2019), *Bulbul* (November 2019), *Amphan* (May 2020), and *Yaas* (May 2021). Flood inundation is a major contributor to high susceptibility and quick changes in the study area's physical and anthropogenic structure because of the severe landing of storm surges. The block-wise rainfall scenario for the years 2010, 2021, and 2022 is also represented in Figure 2.

2.2. Data Sources

The present study was conducted using mainly secondary data and geospatial techniques. The sources of data are mentioned in Table 1. The data used in this study, such as Landsat 8 OLI/TIRS C2 L1, have a spatial resolution of 30 m. The Resourcesat-1/Resourcesat-2 LISS-III has a spatial resolution of 24 m and an AWiFS of 56 m. The data also include rainfall data from 2010 to 2022, as well as the MERRA project collaboration with NASA. There is some uncertainty in the remotely sensed datasets because some data were not available in the same online repositories of Landsat 8/9 or IRS Resourcesat. Therefore, during the three study years, the obtained datasets at the same resolution could not be used. The data used in this study for analysis are outlined in the web links provided.

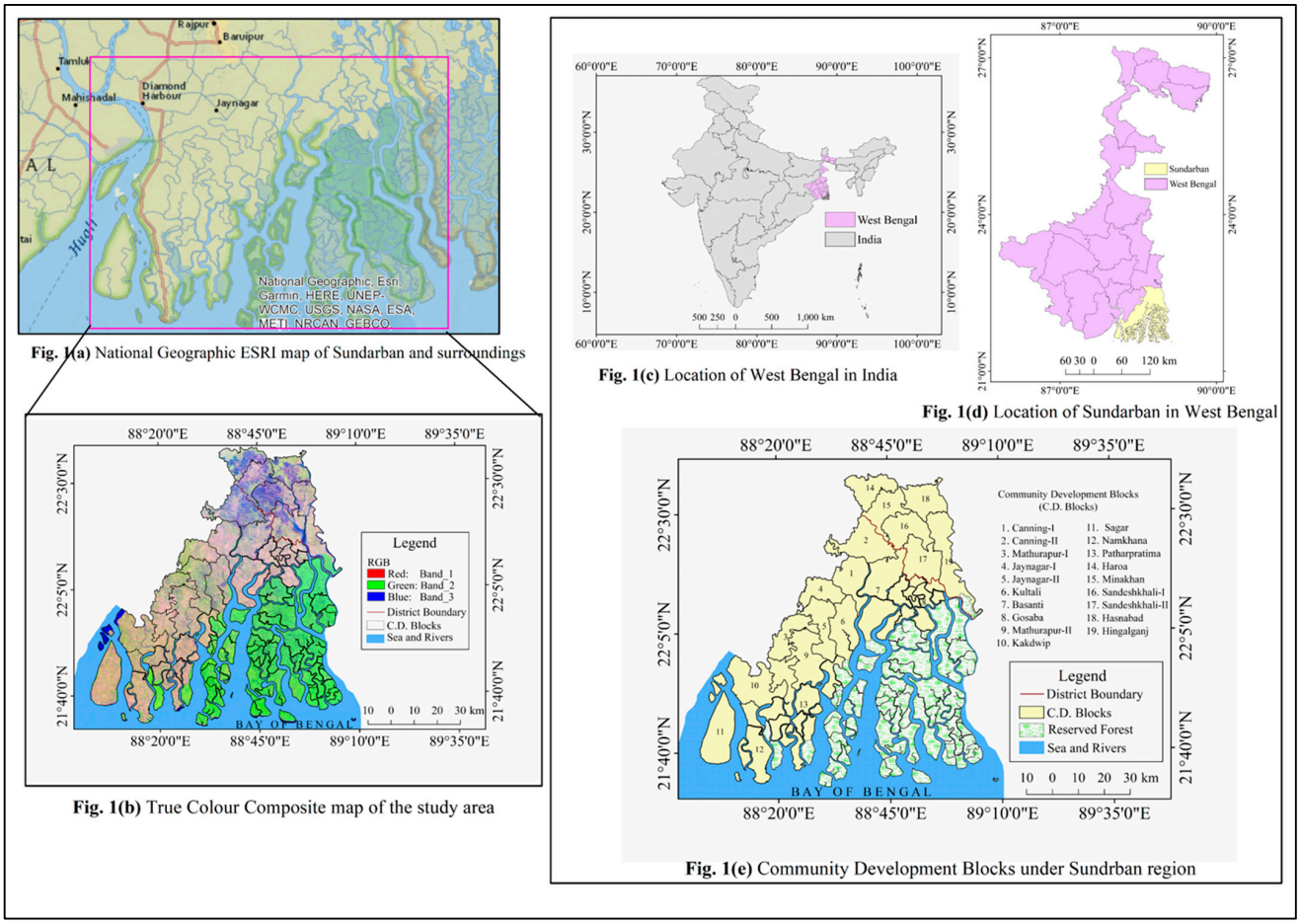


Figure 1. (**a**–**e**) Location map of the study area.

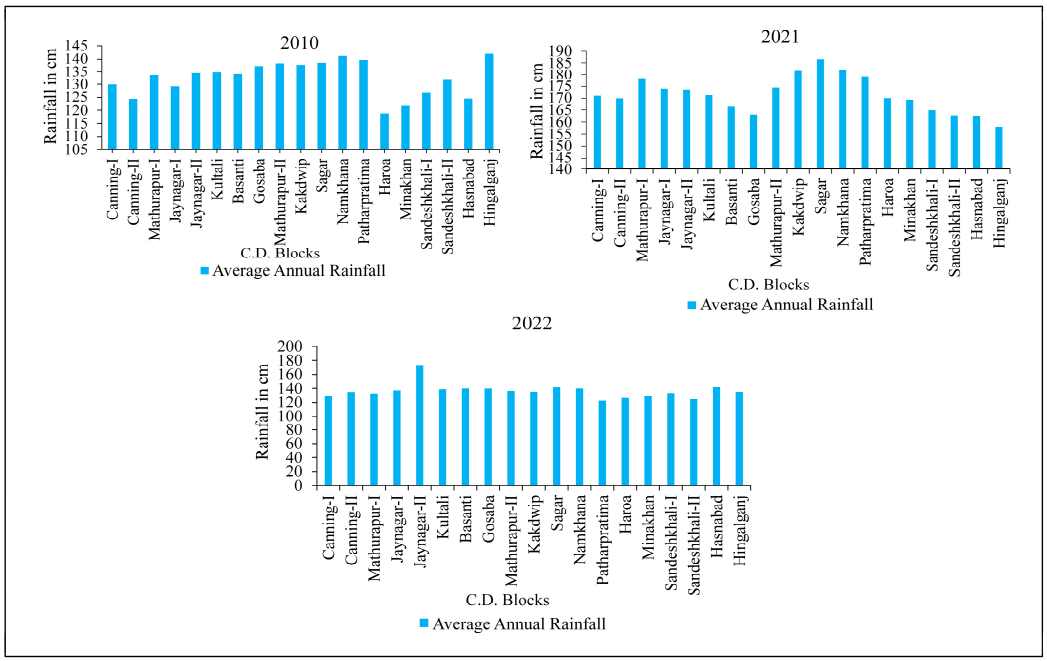


Figure 2. Block-wise distribution of average annual rainfall (cm) in the Sundarbans (2010, 2021, and 2022).

Table 1. Sources and use of available data.

Serial. Number.	Data	Year	Spatial, and Temporal Resolution	Data Sources	Purpose of Data Usage	Website
Category 1: Remote Sensing datasets						
1	Landsat 8 OLI/TIRS C2 L1	2021 (Date Acquired: 21 December 2021; File Date: 29 December 2021); 2022 (Date Acquired: 22 November 2022; Date Product Generated: 29 November 2022	Spatial resolution: 30 m (visible, NIR, SWIR); 100 m (thermal); and 15 m (panchromatic. Temporal resolution: 16 days	[33,34]	To determine the spectral indices	https://earthexplorer.usgs.gov/ (accessed on 26 December 2022)
2	Resourcesat-1/Resourcesat-2: LISS-III (2009, 2016, and 2019) and AWiFS (2010)	Date of Pass: 23 November 2009; 26 December 2010; 20 April 2016; 4 February 2019	Spatial resolution: LISS-III: 24 m; AWiFS: 56 m. Temporal resolution: 5 days	[35–38]	To determine the spectral indices	https://bhuvan-app3.nrsc.gov.in/data/download/index.php (accessed on 22, 23, and 26 December 2022; and 3 January 2023)
Category 2: Rainfall data						
3	Rainfall (cm)	2010, 2021, 2022 (January to December)		[39–44]	To calculate the average annual rainfall	https://mausam.imd.gov.in/ Website of Solar Radiation Data (SODA): Modern-Era Retrospective Analysis for Research and Applications (MERRA) Project collaboration with NASA (https://gmao.gsfc.nasa.gov/reanalysis/MERRA-2/) (Accessed on 23 December 2022, and 6 February 2023)

2.3. Selection of the Indicators (Spectral Indices)

Based on various criteria, six spectral indices—NDVI, MNDWI, NDMI, BSI, NDBI, and NDTI—were analyzed to identify the flood susceptibility zones. In the present study's regression analysis, these were the independent variables that forecasted the normalized difference flood index (NDFI), which was used to identify the zones with the highest likelihood of flooding the study region. The details of the indicators are presented in Table 2. These indexes have been used in various studies to assess the condition of vegetation, water, and built-up areas. Table 2 lists the specifics of the equations as well.

Table 2. Details of the selected spectral indices used as the indicators of flood susceptibility.

Sl. No.	Variables (Indices)	Measurement	Source(s)	Purpose of Selection
1	Normalized Difference Vegetation Index (NDVI)	$NDVI = \frac{NIR-RED}{NIR+RED}$	[45]	The spectral index is used for measuring surface vegetation conditions.
2	Modified Normalized Difference Water Index (MNDWI)	$MNDWI = \frac{Green-SWIR}{Green+SWIR}$	[46]	The spectral index is used for measuring surface vegetation conditions. The spectral index for measuring the enhanced surface water condition.
3	Normalized Difference Moisture Index (NDMI)	$NDMI = (NIR - SWIR)/(NIR + SWIR)$	[47]	The spectral index is used to determine vegetation water content.
4	Bare Soil Index (BSI) *	$BSI = ((Red + SWIR) - (NIR + Blue))/((Red + SWIR) + (NIR + Blue))$	[48–50]	The spectral index indicates soil bareness.
5	Normalized Difference Built-up Index (NDBI)	$NDBI = \frac{SWIR-NIR}{SWIR+NIR}$	[51]	The spectral index for determining habitation (built-up areas) condition.
6	Normalized Difference Turbidity Index (NDTI)	$NDTI = \frac{Red-Green}{Red+Green}$	[52,53]	The spectral index is used to estimate the turbidity in water bodies.

* As the Blue band is not present in LISS-III and AWiFS data, the authors projected the output of BSI (created using Landsat data) for the year 2010.

2.4. Methods and Techniques

The detailed methods and techniques are mentioned in the following subsections with necessary definitions and subsequent citations. Additionally, all the equations concerning the methods and techniques are illustrated in Appendix A.

2.4.1. Spectral Indices and Buffer Creation

A spectral index termed the combined Mangrove Recognition Index (CMRI) [54] Equation (A1), was used to determine the mangrove vegetation's state, and NDWI is a Normalized Difference Water Index denoted as the spectral index for measuring vegetation moisture conditions. The formula of NDWI [55] is mentioned in Equation (A2). A spectral index entitled the Mangrove Damage Indicator (IM) [56] (Equation (A3)) was used to spot damage to mangrove plants. The spectral indices of determining flood conditions are the Normalized Difference Flood Index (NDFI), Normalized Difference Flood Index2 ($NDFI_2$), and Normalized Difference Flood Index3 ($NDFI_3$). As a spectral index of flood conditions, the NDFI highlights the temporary open water bodies and shallow water in short vegetation. The present study adhered to the methods used by the researchers [57,58]. The index values were then subjected to a threshold to extract only the flooded areas. The formulas of $NDFI_2$ and $NDFI_3$ are mentioned in Equations (A4) and (A5), respectively. As the Blue band is not included in LISS-III and AWiFS data, the authors projected the output of BSI (created using Landsat data) for the year 2010. This formula was used for the construction of the NDFI map of 2010. This formula was used for the construction of the NDFI map for 2021 and 2022. Figure 3 shows a general conceptual framework of the methodology of the present study. Randomly, 103 points were extracted in the GIS environment based on the NDFI value and flood condition. The multiple-ring buffer was created according to the distances of 500 m, 1000 m, and 2000 m to visually interpret the flood proximity from each NDFI point.

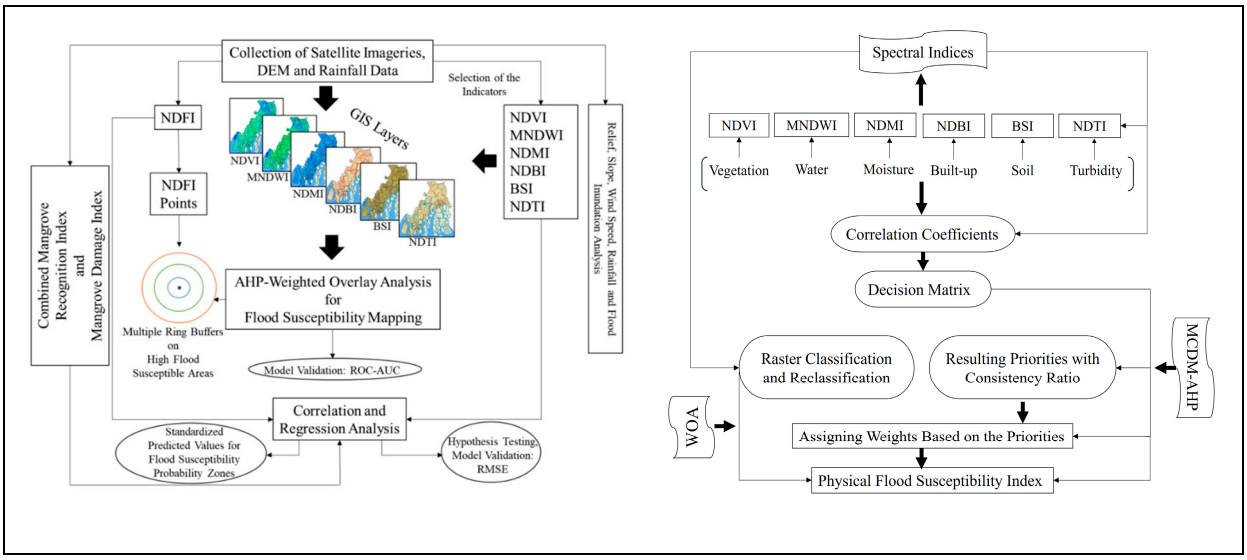


Figure 3. The general methodological framework and logical structure of the technical roadmap of the present study.

2.4.2. Multi-Criteria Decision-Making-Analytical Hierarchy Process (MCDM-AHP), and Weighted Overlay Analysis (WOA) Method

The multi-criteria decision-making (MCDM) process uses the analytical hierarchy process (AHP), a statistical decision-making technique, to calculate a statistical measure of the flood vulnerability index (FVI). This approach was utilized in earlier studies, such as [59–64], to determine the flood vulnerability index and flood susceptibility index. The analytical hierarchy process is a method of measurement based on the dependencies between and within a collection of items [65]. The criteria, sub-criteria, characteristics, and decision-alternative hierarchy are derived first [66]. Based on the computation by Saaty [67], a 9-point scale quantifying preference is then created for the pairwise comparison of each criterion. It is written as $A = [a_{ij}]_{n \times n}$ in the formulation of the pairwise comparison matrix in Equation (A6). The vector of weights, $w = [w_1, w_2, w_3, \ldots, w_n]$, is then determined using Saaty's eigenvector [66] in Equation (A7). The correlation between the variables' determinants was employed in this study to build this matrix. The weights, consistency index, and consistency ratio were calculated using the formulae shown in Equation (A8), Equation (A9), and Equation (A10). By dividing the consistency index (*CI*) by the random index suggested in [65], it was possible to calculate the consistency ratio (*CR*) of the pairwise comparison in the AHP process. The acceptable consistency ratio was $\leq$0.10, and the inadequate consistency ratio was $\geq$0.10 [65]. A random index (*RI*) was made up of six elements that were measured and cited [68,69] and was regarded in the current investigation to be 1.54. The authors' observations of the on-site scenarios and the assigned correlation matrix of the relationships among the indices were used to calculate the resulting priorities The decision matrix was used to determine the indices' priorities. The input of each determined weight associated with the criteria in the weighted overlay analysis of the GIS environment yields the flood vulnerability assessment (composite flood susceptibility index), based on the research [70] of the C.D. Blocks in the study area in the final phase. For the composite flood susceptibility index of the selected study area, five categories—very high, high, moderate, low, and very low—of flood susceptibility were recognized. A weighted overlay analysis was assigned here following the techniques used by various studies, including [71–77], to determine the flood vulnerability and susceptibility in GIS, specifically in coastal and cyclone-prone areas. According to its definition, weighted overlay is an approach to modeling suitability. To obtain an output value, the value of each raster cell is multiplied by the layer weight, and the values are added together [73]. The following formula was adopted for analyzing weighted overlay in Equation (A11).

2.4.3. Statistical Analyses

Descriptive statistics were applied to obtain the value of the mean and standard deviation (SD) of the selected variables used in this study. A multiple linear regression model was utilized to forecast the NDFI based on the chosen flood susceptibility characteristics. The Durbin–Watson statistic (DW statistic) [78] was also retrieved in the regression model to help explain the type of autocorrelation among independent variables and the validity of the model. The analysis of the multiple linear regression model embraced significance tests and the analysis of variance (ANOVA) [79] in addition to the coefficients of determinants. The resultant standardized predicted values (ZPR values) were also retrieved for the prediction of the flood susceptibility zones in the study areas. The formula of the multiple linear regression model (multivariate regression model) [80] is mentioned in Equation (A12). Equation (A13) or Equation (A14) was used to compute the F value in the *j*th one-way ANOVA to determine the F-statistics [79]. The explained variance, or between-group variability, is illustrated in Equation (A15), and the 'unexplained variance', or 'within-group variability', is illustrated in Equation (A16). This F-statistic follows the F-distribution with K-1, N-K degrees of freedom (df) under the null hypothesis. To estimate the model validation by measuring the error to predict the data, the root mean square error (RMSE) [81] method was used. The formula of RMSE is mentioned in Equation (A17).

To test the hypotheses, a two-sample t-test with unequal variance was performed. In this case, data from two statistical populations were used to evaluate the hypothesis (variable 1: NDFI; variable 2: IM). Welch's *t*-test [82] is mentioned in Equation (A18).

During hypothesis testing, the following are plausible:

Null hypothesis (H_0): The mangrove index (IM) and the flood index (NDFI) do not significantly correlate $\mu 1 = \mu 2$ (when the null hypothesis shows that the means of the two statistical populations are equal).

Alternative hypothesis (H_1): The mangrove index (IM) and the flood index (NDFI) have a substantial inverse relationship, $\mu 2 \neq \mu 1$ (when the alternative hypothesis shows that there is a difference between the means of the two statistical populations). A 95 percent confidence interval was used in the analysis of Welch's degrees of freedom.

2.4.4. Model Validation

The present study adopted the model validation techniques proposed in the previous studies [83,84]. The flood susceptibility index model in the study region was validated using a receiver operating characteristic (ROC) curve and area under the ROC curve (AUC) for the years 2010, 2021, and 2022. The probability was visually represented using the ROC curve, and the area under the ROC curve (AUC) was calculated using the true positive rate of 1-sensitivity and the false positive rate of specificity.

3. Results

3.1. Major Cyclonic Events from 2009 to 2021

The following tropical cyclones were the major outbursts over the Indian Sundarbans: *Aila* (May 2009), *Komen* (July 2015), *Fani* (April–May 2019), *Bulbul* (November 2019), *Amphan* (May 2020), and *Yaas* (May 2021). The Indian Meteorological Department (IMD) [85–89] reported the details of the cyclones, including their origin, track, disastrous activities, early warning, and management strategies in different phases of the cyclones. The Indian Sundarbans region has been severely impacted by various cyclones, including the powerful cyclone *Aila* between 23 May and 26 May 2009, which caused significant damage to the Bay of Bengal. The storm resulted in 2.2 million people being displaced, with over 132,000 homes suffering partial damage and 61,000 completely collapsing. The cyclonic storm *Komen* began as a low-pressure area on July 25 and moved into neighboring Bangladesh and Gangetic West Bengal before condensing into a depression on 26 July. The extremely severe cyclonic storm (ESCS) *Fani* began on 26 April and persisted until May 4 over the southeast Bay of Bengal and east central equatorial Indian Ocean. It led to the devastation of 16,309 villages, 83 deaths, 10,088 animals killed, and 107,808 homes

destroyed. Super cyclonic storm *Amphan* moved 15 km/h north-northeast on 19 May 2020 and was expected to move north-northeasterly across the northwest Bay of Bengal and the coasts of Bangladesh and West Bengal between Digha (West Bengal) and the Hatiya Islands (Bangladesh), not far from the Sundarbans. Very severe cyclonic storm *Yaas* traveled north-northwestward across the northwest Bay of Bengal on 26 May 2021, at a speed of roughly 15 km/h. Heavy to very heavy rainfall was observed in some isolated locations, and gale winds with gusts up to 110 km/h were blowing along and off the coast of the state. Fishing operations, ship movements, evacuation, rail and road traffic control, and preparations for future cyclones have been made.

3.2. Physical Susceptibility to Flood in Sundarbans

A total of six spectral indices (Table 3) were chosen to determine the physical susceptibility of Sundarbans flood events in 2010, 2021, and 2022 due to cyclonic storms (post-cyclonic periods of *Aila*, *Amphan*, and *Yaas*). The NDVI, MNDWI, NDMI, NDBI, BSI, NDTI (predictors), and NDFI are the chosen indices (predicted variables). The mean and standard deviation of the selected predictors of physical susceptibility to flooding are represented in Table 3. In 2010, the highest mean value among the six indices was in the case of NDVI (0.2288) and the SD value in the case of NDMI (0.1626) and NDBI (0.1626). In 2021, the highest mean value was followed in the case of NDMI (0.1114) and the SD value in the case of NDBI (0.0689). In 2022, the highest mean value was followed in the case of NDVI (0.1865) and the SD value in the case of NDVI (0.08951). The maps of NDVI, MNDWI, NDMI, NDBI, BSI, and NDTI (2010, 2021, and 2022) are represented in Figures A1 and A2 in Appendix B, respectively.

Table 3. Descriptive statistics of the selected variables (2010, 2021, and 2022).

Variables	2010		2021		2022	
	Mean	**Std. Deviation**	**Mean**	**Std. Deviation**	**Mean**	**Std. Deviation**
NDVI	0.2288	0.11714	0.1006	0.06134	0.1865	0.08951
MNDWI	−0.2030	0.12920	0.0403	0.06208	−0.0745	0.07501
NDMI	−0.0688	0.16263	0.1114	0.06887	0.1014	0.05465
NDBI	0.0688	0.16263	−0.1112	0.06896	−0.1014	0.05465
BSI	0.0058	0.11480	−0.0953	0.04032	−0.0407	0.03938
NDTI	−0.0958	0.03548	−0.0294	0.00999	−0.0132	0.01450
NDFI	−0.2925	0.11391	0.0898	0.07128	−0.0572	0.05385
Valid N (listwise): 19						

Based on the geospatial analysis and AHP-weighted overlay analysis method, the zones of physical susceptibility to flooding were delineated for the years 2010, 2021, and 2022. Table A1 (in Appendix C) shows the classification and reclassification of raster layers for weighted overlay analysis. The weights were calculated using the MCDM-AHP method, in which the consistency ratio (CR) is acceptable (3.3%, Table 4). Nine classes and those reclassified were identified concerning the selected indices, and their weights were also assigned. As per the calculation, NDVI has the highest priority (45.7%), and NDTI has the lowest (3.6%). This study utilized Saaty's Random Index table for the calculation of the consistency ratio. Figure 4 shows the physical susceptibility zones of the flood of the Sundarbans in 2010, 2021, and 2022. The overall flood susceptibility was very high in the north-eastern riverine areas and south-western coastal areas of the study area, consisting of Sandeshkhali-I and II, Kakdwip, and islets under the Sagar block. The temporal situation of flood susceptibility varied in 2010, 2021, and 2022. Based on the flood susceptibility mapping, low susceptibility was observed mostly in the northern and western portions of the study area in 2010, which changed to moderate and moderate to low in 2021 and 2022, respectively. The ROC-AUC analysis was used to verify the WOA model (Figure 5). The AUC's overall accuracy ranged from 79.5 percent in 2010 to 77.7 percent in 2021 to

77.4 percent in 2022. The values of the area of the fitted ROCs, which ranged from 0.705 to 0.777, were good and fell within an acceptable range. These are the resulting weights for the criteria based on the pairwise comparisons in Table 4 based on the decision matrix in Table 5.

Table 4. Resulting priorities (base year: 2010; target year: 2022).

Serial Number	Categories	Priority	Rank	(+)	(−)
1	NDVI	45.70%	1	10.70%	10.70%
2	MNDWI	18.80%	3	5.70%	5.70%
3	NDMI	20.70%	2	6.50%	6.50%
4	NDBI	6.90%	4	1.80%	1.80%
5	BSI	4.30%	5	1.50%	1.50%
6	NDTI	3.60%	6	0.90%	0.90%
Number of Comparisons = 15 Consistency Ratio (CR) = 3.3%					
Random Index (RI)					

n	1	2	3	4	5	6	7	8	9	10	11	12
RI	0	0	0.52	0.89	1.11	1.25	1.35	1.4	1.45	1.49	1.51	1.54

AHP Scale: 1—Equal Importance, 3—Moderate Importance, 5—Strong Importance, 7—Very Strong Importance, 9—Extreme Importance (2,4,6,8 values in-between). Source: [68].

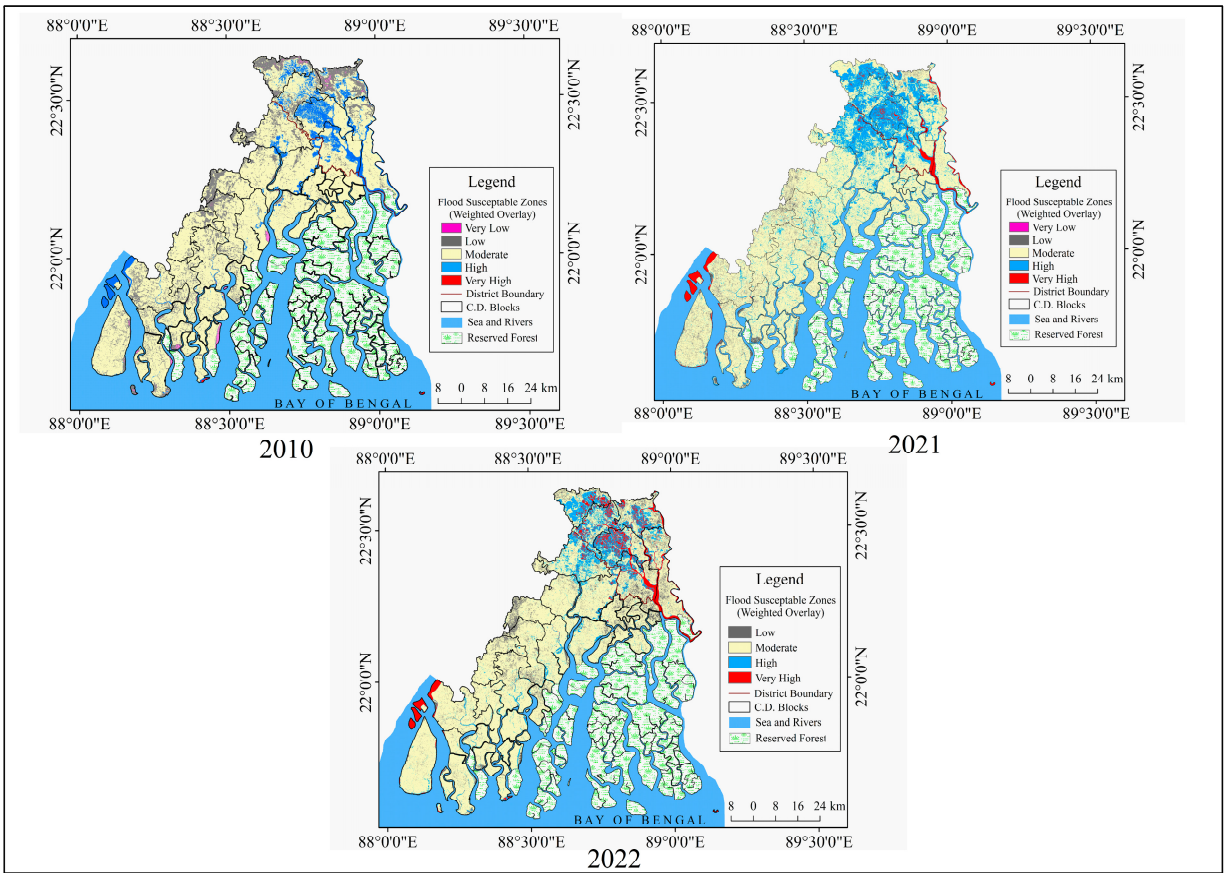


Figure 4. Flood susceptibility zones of Sundarbans (2010, 2021, and 2022).

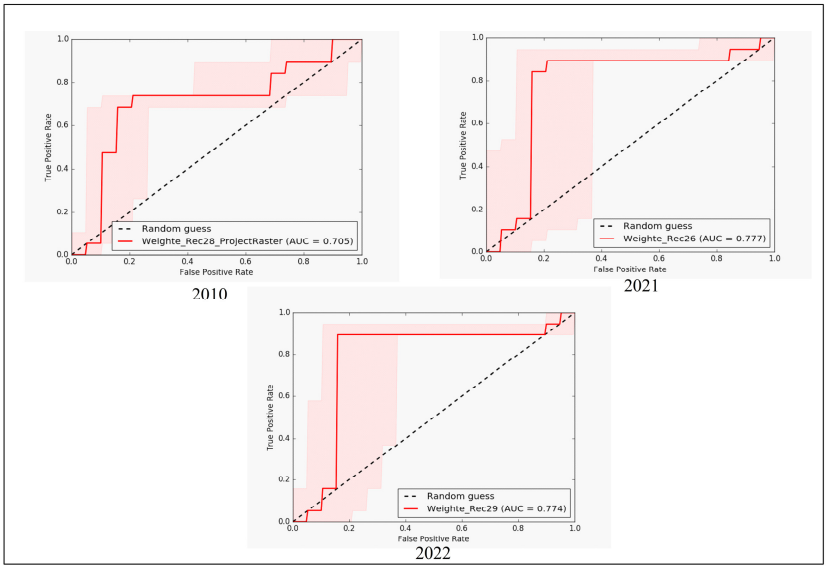


Figure 5. ROC-AUC for model validation (2010, 2021, and 2022).

Table 5. Decision matrix (base year: 2010; target year: 2022).

Decision matrix						
	1	2	3	4	5	6
1	1	3.00	3.00	7.00	9.00	9.00
2	0.33	1	1.00	2.00	7.00	5.00
3	0.33	1.00	1	5.00	5.00	5.00
4	0.14	0.50	0.20	1	2.00	2.00
5	0.11	0.14	0.20	0.50	1	2.00
6	0.11	0.20	0.20	0.50	0.50	1

Principal eigen value = 6.206. Eigenvector solution: 4 iterations, delta = 0.0000000290.

3.3. Relationship of NDFI with the Indicators of Flood Susceptibility

The present study identified the relationship between NDFI and indicators of flood susceptibility, which varied over time (2010, 2021, and 2022, Table 6). The MNDWI had a highly and significantly positive relationship with NDFI (r values were 0.963 in 2010, 0.911 in 2021, and 0.923 in 2022; $p < 0.05$), and the lowest relationships were found concerning the NDTI (r value was −0.155, $p > 0.05$) in 2010; NDVI (r value was −0.300, $p > 0505$) in 2021; and BSI (r value was −0.302, $p > 0.05$) in 2022. Table A2 (in Appendix C) shows the output of the linear regression model. The Durbin–Watson value was in an acceptable range but was less than 2.0. This indicates a slight positive autocorrelation, which excludes the MNDWI and NDMI. Thus, the present study predicted the NDFI values with NDVI, NDBI, BSI, and NDTI and compared the results with the previous AHP-WOA analysis of flood susceptibility. The overall prediction value of the independent variables was 94.0%, which is significant also ($p < 0.005$). The low RMSE value (0.003) indicates that the model fits the data well. The unstandardized coefficients concerning NDVI, NDBI, BSI, and NDTI were −0.658 ($p < 0.05$), −0.797 ($p > 0.05$), −0.168 ($p > 0.05$), and −0.709 ($p > 0.05$), respectively. These values indicate that a 1 unit increase in NDVI significantly decreased 65.8% of the NDFI. The rest of the indicators were not statistically significant.

Table 6. Correlation between NDFI and indicators of flood susceptibility (2010, 2021, and 2022).

2010		**NDFI**	**NDVI**	**MNDWI**	**NDMI**	**NDBI**	**BSI**	**NDTI**
Pearson Correlation [90,91]	NDFI	1.000	−0.175	0.963	0.641	−0.641	−0.643	−0.155
* Sig. (1-tailed)		.	0.237	0.000 *	0.002 *	0.002 *	0.001 *	0.264
2021								
Pearson Correlation	NDFI	1.000	−0.300	0.911	0.665	−0.663	−0.651	−0.625
Sig. (1-tailed) *		.	0.106	0.000 *	0.001 *	0.001 *	0.001 *	0.002 *
2022								
Pearson Correlation	NDFI	1.000	−0.448	0.923	0.364	−0.364	−0.302	−0.621
Sig. (1-tailed) *		.	0.027 *	0.000 *	0.063	0.063 *	0.104	0.002 *

* 95% Confidence Interval ($p < 0.05$).

Table A3 (in Appendix C) shows the block-wise variation of the NDFI and ZPR values of flood susceptibility probability in the study area in 2010, 2021, and 2022. In Figure 6, NDFI maps are represented, along with the selected NDFI-based flood points on the map in Figure 7. The 500 m, 1000 m, and 2000 m multi-buffer rings were created based on the NDFI points to visually interpret the proximity of flood occurrences (Figure 7). In 2010, the highest and lowest values of NDFI were found in the blocks of Sandeshkhali-II (−0.07027) and Canning-I (−0.45946), respectively. The highest and lowest ZPR values this year were in Haroa (2.78633) and Mathurapur-I (−1.13422), respectively. In 2021, the highest and lowest NDFI and ZPR values were found in the blocks of Mathurapur-II (0.238038) and Mathurapur-I (−0.03463); Haroa (2.78633); and Mathurapur-I (−1.13422), respectively. In 2022, the highest and lowest NDFI and ZPR values were found in the blocks of Haroa (0.093731) and Minakhan (−0.12439); Sandeshkhali-II (1.94128); and Canning-I (−1.46359), respectively. The relationship between NDFI and ZPR was positive in 2022 (Figure 8). A highly predicted susceptibility probability of flood was found in most of the riverine, built-up, and marshy land areas of the Sundarbans in 2010, 2021, and 2022 (Figure 8). Finally, classes of AHP-weighted overlay analysis are compared with ZPR classes in Table 7, where the percentages of very low, low, moderate, high, and very high category flood susceptible areas were 19.84, 22.12, 52.00, 5.99, and 0.05, respectively, in 2010. Similarly, the percentages of very low, low, moderate, high, and very high category flood susceptible areas were 0.00103, 12.70, 71.72, 13.44, and 2.13 in 2021, and the percentages of low, moderate, high, and very high category flood susceptible areas were 9.51, 76.59, 9.25, and 4.65 in 2022. The highly susceptible flood areas were reduced in 2022 from the years 2010 and 2021. Recent mangrove plantation and flood management activities have had a significant impact on reducing the physical susceptibility of floods and flood susceptibility probabilities.

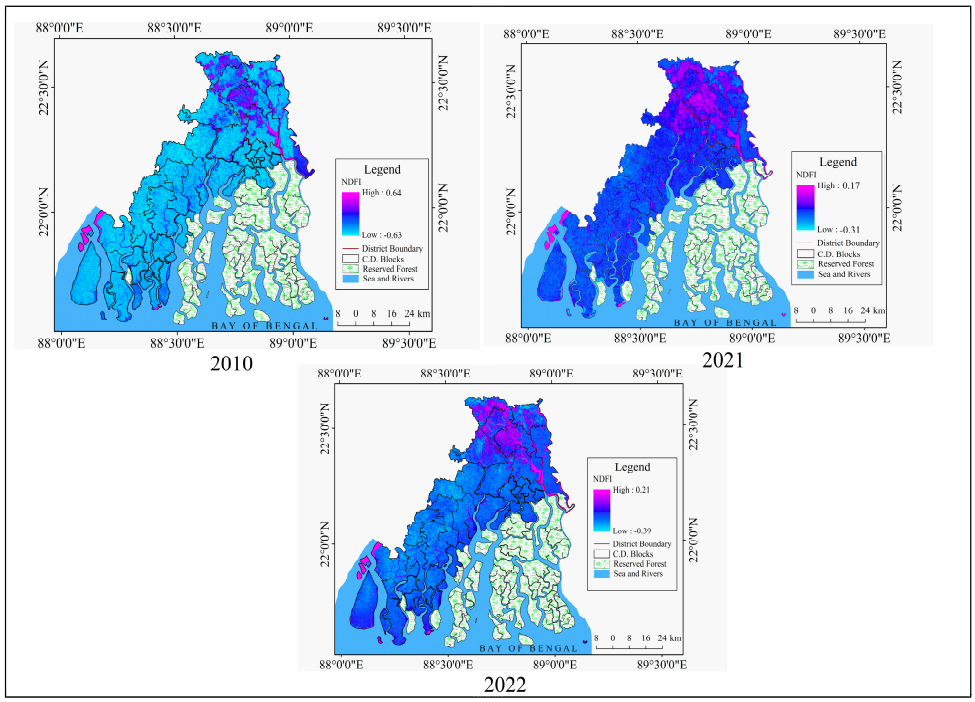


Figure 6. NDFI maps of the Sundarbans (2010, 2021, and 2022).

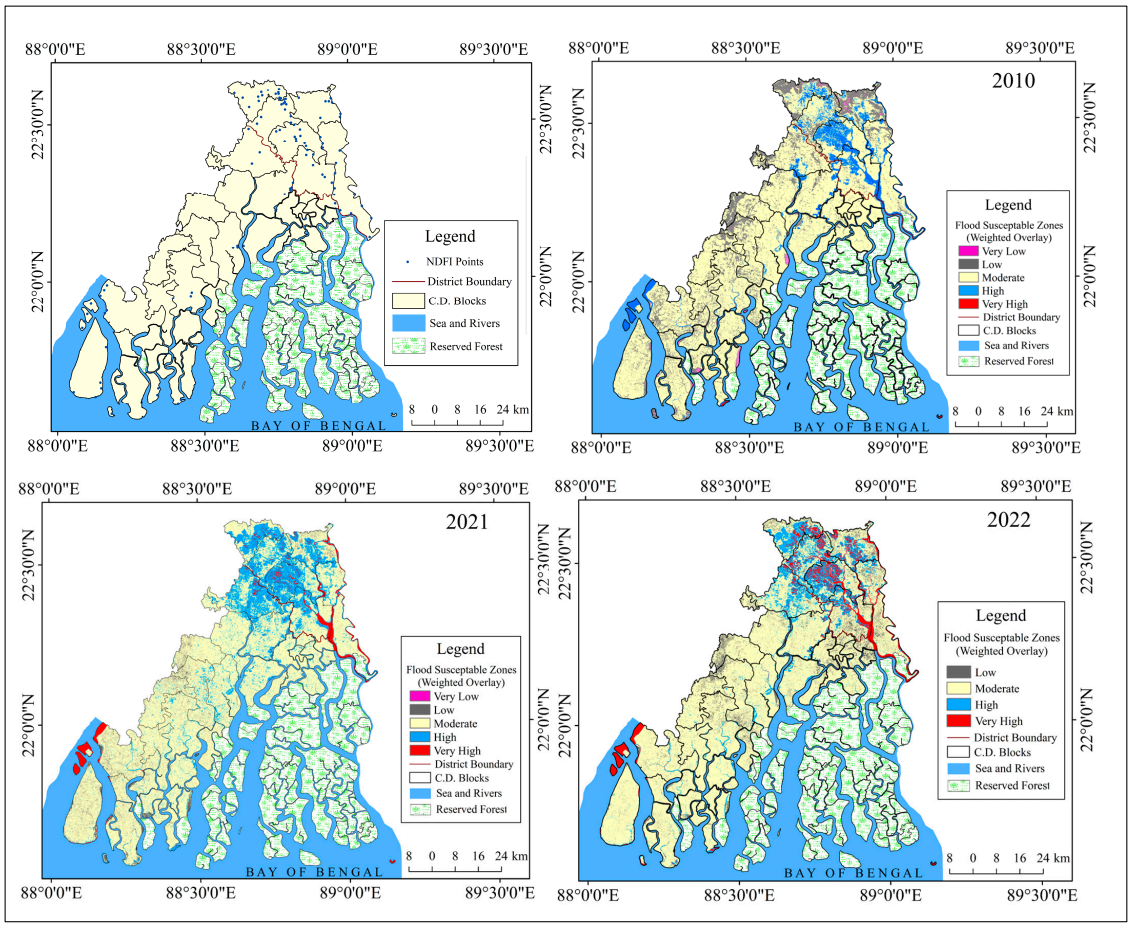


Figure 7. Selected points based on NDFI (2022) and NDFI point buffer areas in the flood susceptibility map of the Sundarbans (2010, 2021, and 2022).

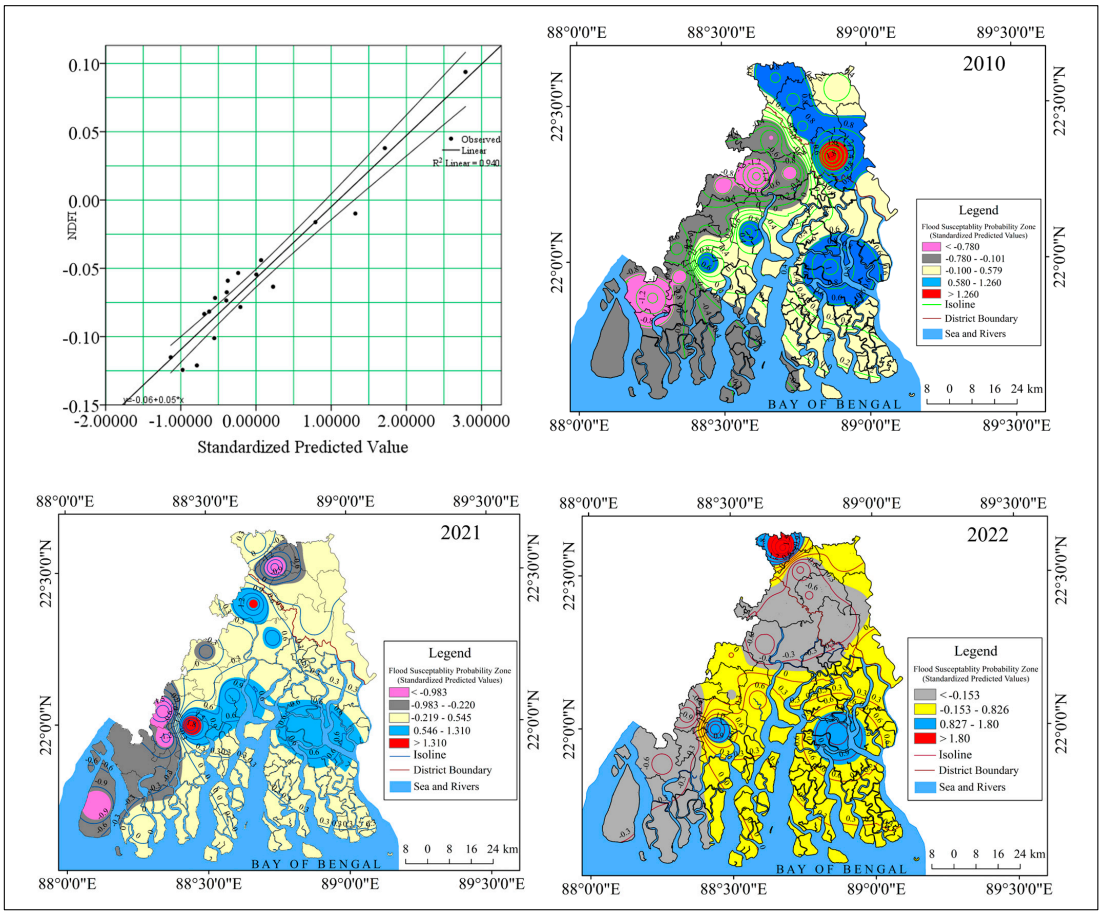


Figure 8. Relationship between NDFI and standardized predicted value (ZPR) (2022) and flood susceptibility probability zones of the Sundarbans (2010, 2021, and 2022).

Table 7. Categorization of flood susceptibility and flood susceptibility probability zones.

Year	Weighted Overlay Classes	Categories	Area (%)	ZPR Classes	Categories
2010	3	Very Low	19.84	<−0.780	Very Low
	4	Low	22.12	−0.780–−0.101	Low
	5	Moderate	52.00	−0.100–0.579	Moderate
	6	High	5.99	0.580–1.260	High
	7	Very High	0.05	>1.260	Very High
2021	3	Very Low	0.00103	<−0.983	Very Low
	4	Low	12.70	−0.983–−0.220	Low
	5	Moderate	71.72	−0.219–0.545	Moderate
	6	High	13.44	0.546–1.310	High
	7	Very High	2.13	>1.310	Very High
2022	4	Low	9.51	<−0.153	Low
	5	Moderate	76.59	−0.153–0.826	Moderate
	6	High	9.25	0.827–1.80	High
	7	Very High	4.65	>1.80	Very High

3.4. Changes in Mangrove Area

The present study identified the combined mangrove recognition index (CMRI) and mangrove damage index (IM) from the years 2009 to 2022 in the Sundarbans (Figures A3 and A4 in Appendix B and Figure 9). CMRI ranged from −0.64 (low) to 0.93 (high) (2009), −0.64–0.91 (2010), −0.53–0.76 (2016), −0.52–0.85 (2019), −0.32–0.66 (2021), and −0.34–0.62 (2022). Except for the Sundarbans Biosphere Reserve, the highest index of mangrove vegetation was recognized in the C.D. block named Gosaba (0.929 in 2009), 0.908 (2010), 0.553 (2016), 0.844 (2019), 0.431 (2021), and Mathurapur-I (0.419 in 2022). The lowest index of mangrove vegetation was recognized in the C.D. block named Sandeshkhali-II (0.005 in 2009; 0.024 in 2010), Haroa (−0.061 in 2016), Mathurapur-II (−0.521 in 2019; −0.038 in 2021), and Haroa (−0.138 in 2022). The area of dense mangrove vegetation coverage in the total area of the Sundarbans increased from 31 percent to 37 percent (2009–2010) and subsequently decreased to 31 percent, 28 percent, and 30 percent in 2016, 2019, and 2021, respectively. The mangrove area also increased to 41 percent in 2022 due to the large-scale governmental and non-governmental initiatives of the mangrove plantation programs. However, the overall mangrove damage showed an increasing trend from 2009 to 2022. The mangrove forest was less affected in the SBR area than in other portions of the Indian Sundarbans.

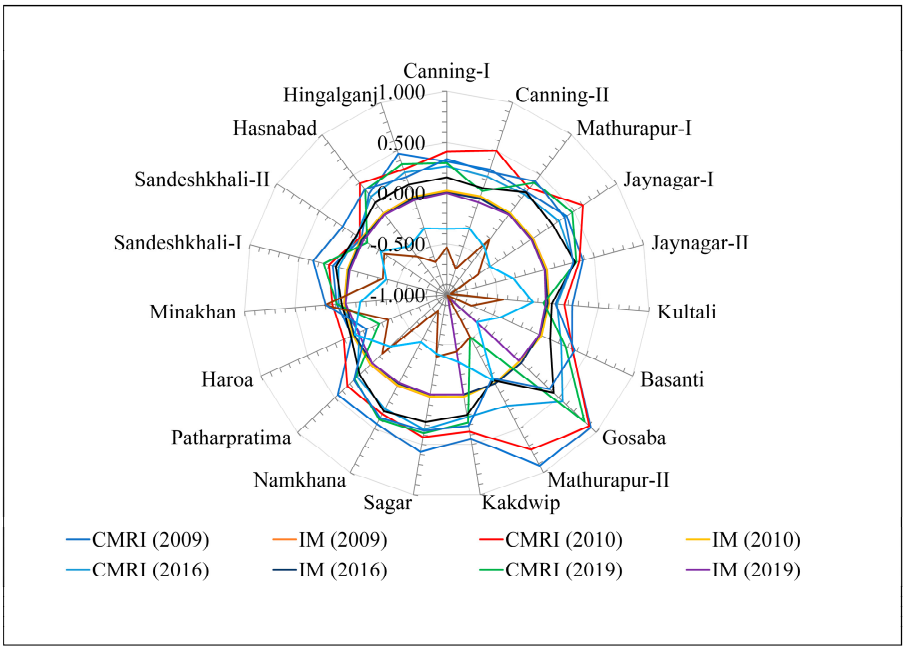


Figure 9. Variation of CMRI and IM (2009, 2010, 2016, 2019, 2021, and 2022).

3.5. Results of Hypothesis Testing

Table 8 presents the findings of the hypothesis testing. The differences between the two population means and standard errors in this instance were calculated in 2022 as 0.257957 and 0.035556, respectively. The estimated t value was 7.2549 (Welch's degrees of freedom = 23.2374) with a 0.05 significance level, since it was assumed that the difference = mean (NDFI)-mean (IM) where H0: difference = 0 is equal to zero. Pr (|T| > |t|) = 0.0000 based on the alternative hypothesis, Ha: diff! = 0. The *p*-value was less than 0.05. This demonstrates that the mean difference was statistically distinct from zero (a two-tailed test). According to the results, flooding significantly contributes to mangrove vegetation degradation in the Indian Sundarbans.

Table 8. Results of the hypothesis test (2022).

Two-Sample *t* Test with Unequal Variances (Unpaired Unequal Welch's Test)						
Variables	Obs [1]	Mean	Std. Err. [2]	Std. Dev. [3]	[95% Conf.	Interval] [4]
NDFI	19	−0.0563158	0.0121927	0.0531466	−0.0819316	−0.0306999
IM	19	−0.3142728	0.0334002	0.1455879	−0.3844439	−0.2441017
combined	38	−0.1852943	0.0275159	0.1696192	−0.2410467	−0.1295419
diff		0.257957	0.035556		0.1844453	0.3314687
diff [5] = mean (NDFI)-mean (IM) t = 7.2549 H_0: diff = 0 Welch's degrees of freedom = 23.2374						
H_a: diff < 0 Pr(T < t) = 1.0000			H_a: diff! = 0 Pr(|T| > |t|) = 0.0000			H_a: diff > 0 Pr(T > t) = 0.0000

[1] Obs = Number of observations (or cases); [2] Std. Err. = Standard error; [3] Std. Dev. = Standard deviations; [4] Conf. Interval = Confidence interval; [5] diff = Difference in differences.

4. Discussion

Super cyclones and the accompanying floods, particularly *Aila* in 2009 and *Amphan* in 2021, have devastatingly damaged the mangrove ecosystem in the Sundarbans region, which is essential for Bangladesh and India. Climate change is predicted to put more stress on mangrove forests, which would lower millions of people's standards of living in developing countries [22]. Super cyclone *Amphan* in the Sundarbans region of South Asia raises concerns about how to manage numerous disasters while preserving ecosystems [14]. Significant cyclonic events, including massive outbursts like *Aila*, *Komen*, *Fani*, *Amphan*, and *Yaas*, occurred in the Indian Sundarbans between 2009 and 2021. Some field scenarios are represented in the Appendix section (Appendix B: Figure A5a–p). Across and off the state's coast, cyclonic winds with gusts of up to 110 km/hour affect West Bengal's South Twenty-Four Parganas districts. During the assessment of the flood's physical susceptibility, six variables, including NDVI, MNDWI, NDMI, NDBI, BSI, and NDTI, were analyzed. There was evidence of extremely high and high susceptibility in the north-eastern riverine and south-western coastal sections of the Sundarbans. A portion of these areas is also highly susceptible to flooding. This study evaluated the Sundarban Biosphere Reserve's susceptibility to storm surge floods in Indian villages using a composite vulnerability index. Since nearly half of the 1063 localities have insufficient resilience, it is advantageous for local officials to reduce and adapt to storm surge flood dangers [25]. Based on the NDVI, NDBI, BSI, and NDTI, the included coefficients in the present study show the highest influence of vegetation (NDVI) on flood occurrences (NDFI). The overall accuracy of the AUC varied between 79.5 and 77.7 percent between 2010 and 2022. A coastal vulnerability index was created to assess the level of danger within the Sundarban Biosphere Reserve. The vulnerability index was used to categorize the 754 km of shoreline into three groups: high, moderate, and low. This method can be used to create a comprehensive strategy for managing and protecting coastal environments [28]. Restoration efforts are also guided by radar-based inundation analysis [15]. The Indian Sundarbans face environmental challenges from sea level rise, cyclone landfall, and sediment starvation. In 2022, there was a negative correlation between the NDFI and the NDVI. It showed that a greater amount of vegetation can lessen the study area's physical vulnerability to flooding. The Sundarbans Biosphere Reserve's land use and land cover changes between 1975 and 2006 were examined by [92]. The findings indicated a decline in open mangrove stands and the corresponding biodiversity but an increase in dense mangroves. Over time, an estimated 0.42 percent of the initial mangrove cover has disappeared. In [93], they used Landsat imagery to study changes in land use and land cover in the Sundarbans over the previous 45 years. Using the LULC classification method, characteristics such as arid land, water bodies, sparse forests, moderate forests, and dense forests were assigned. The mangrove damage index (IM) and combined mangrove recognition index (CMRI) for the Sundarbans

were calculated in this present study between 2009 and 2022. The analysis showed that, with a mean difference of 23.2374, flooding significantly contributes to the decline of mangrove vegetation in the Indian Sundarbans. Storm surges consequently produced high-level floods during cyclonic storms on the mainland, having the opposite effect. To differentiate between mangroves and non-mangrove vegetation, the researchers in [54] developed an enhanced index by merging data from NDVI and NDWI. Research shows that between 2000 and 2020, 81 square km of new mangroves were added by plantation and regeneration, while 110 square km was lost to erosion. To understand the nature and extent of the impact of the cyclone and associated hazards across the entire blocks at various locations distributed throughout the study blocks, a close examination of the nature of erosion, damages to the vegetation cover, measurement of erosion, collapse of embankments, household collapse, and related scenarios was required (as shown in Figure A5a–p in Appendix B). It was observed that every year, almost, all the devastating effects of attacks such as *Aila*, *Bulbul*, *Amphan*, *Yaas*, and others severely damaged and degraded the earthen embankment and open mangroves.

5. Conclusions

Climate change has increased the likelihood of natural disasters, particularly tropical cyclones, which threaten the survival of defenseless people. The present study determined the physical susceptibility of floods in the post-*Aila* (2009–2010), post-*Amphan* (2020–2021), and post-*Yaas* (2021–2022) periods using remotely sensed data, a multi-criteria decision-making process, a GIS model-building approach, and statistical analyses. The study found that riverine and coastal areas in the northeast and southwest were highly susceptible to floods. A positive correlation was found between flood susceptibility indicators and NDFI. The study concluded that cyclonic floods significantly impact the decline of mangrove vegetation. Establishing mangrove plantations and flood control measures significantly decreased flood susceptibility. Disaster risk reduction is crucial, and erosion-prone areas and mangrove plantations need to be maintained first. In [94], they discussed people's collective efforts to lessen disasters in the Indian Sundarbans islands. Indigenous knowledge of the area and education can help people take the appropriate safety measures and heal faster. Concerning this, there are amplified early warning systems, storm and flood risk assessments, and surveillance in the cyclone-prone areas of the Sundarbans. According to the study [95], prompt evaluation of cyclones' effects on coastal ecosystems is necessary for successful rescue and recovery efforts. Appropriate planning and protection measures are needed to safeguard the coastal ecosystem and livelihoods [96]. The futuristic goal is to enhance an economy and culture that can withstand natural disasters by reducing risk factors, improving preparedness for cyclones and floods, and utilizing knowledge, innovation, and education. This includes providing housing shelters and humanitarian aid to those affected by cyclonic flood disasters.

Author Contributions: Conceptualization, B.K.M.; methodology, B.K.M., S.M., T.B. and R.D.; software, B.K.M., T.B., S.M. and R.D.; validation, B.K.M., K.A., M.S.F. and S.P.; formal analysis, B.K.M., T.B., S.M., R.D. and R.P.; investigation, B.K.M., T.B. and S.M.; resources, B.K.M., T.B., S.M., R.D. and R.P.; data curation, B.K.M., T.B. and S.P.; writing–original draft preparation, B.K.M., T.B., S.M. and R.D.; writing–review and Editing, B.K.M., T.B., S.M., R.D., R.P., K.A., M.S.F. and S.P.; visualization, T.B., R.D. and S.M.; supervision, B.K.M.; project administration, B.K.M.; funding acquisition, B.K.M., K.A. and M.S.F. All authors have read and agreed to the published version of the manuscript.

Funding: Deep thanks and gratitude to the Researchers Supporting Project (RSP2024R351), King Saud University, Riyadh, Saudi Arabia, for funding this research article. The authors would also like to extend thanks and appreciation to the Indian Council of Social Science Research (ICSSR-MOST (Taiwan)/RP-1/2022-1C) for providing financial support and to Netaji Subhas Open University for ensuring supportive research facilities for the research work.

Institutional Review Board Statement: Not applicable.

Informed Consent Statement: Not applicable.

Data Availability Statement: Due to the nature of this research, participants of this study did not agree for their data to be shared publicly; thus, supporting data are not available.

Acknowledgments: Deep thanks and gratitude to the Researchers Supporting Project number (RSP2024R351), King Saud University, Riyadh, Saudi Arabia, for funding this research article. The authors would like to thank the United States Geological Survey (USGS), National Remote Sensing Centre (NRSC) of India, Indian Council of Social Science Research (ICSSR), SoDA: MERRA Project collaboration with NASA, and India Meteorological Department (Kolkata) for providing necessary and supporting data used in the research work.

Conflicts of Interest: No potential conflicts of interest were reported by the authors.

Abbreviations

SMF	Sundarbans Mangrove Forest
UNESCO	United Nations Educational, Scientific and Cultural Organization
km	Kilometer
mm	Millimeter
cm	Centimeter
TC	Tropical Cyclone
Radar	Radio Detection And Ranging
LiDAR	Light Detection and Ranging
NDVI	Normalized Difference Vegetation Index
SVM	Support Vector Machine
SBR	Sundarban Biosphere Reserve
CVI	Coastal Vulnerability Index
NDFI	Normalized Difference Flood Index
C.D. Blocks	Community Development Blocks
ISR	Indian Sundarban Region
OLI	Operational Land Imager
TIRS	Thermal Infrared Sensor
LISS	Linear Imaging and Self Scanning Sensor
AWiFS	Advanced Wide Field Sensor
MERRA	Meteorological Re-analysis
NASA	National Aeronautics and Space Administration
NIR	Near Infrared
SWIR	Shortwave Infrared
USGS	United States Geological Survey
NRSC	National Remote Sensing Centre
GMAO	Global Modeling and Assimilation Office
SoDA	Solar Radiation Data
MNDWI	Modified Normalized Difference Water Index
NDMI	Normalized Difference Moisture Index
BSI	Bare Soil Index
NDBI	Normalized Difference Build-up Index
NDTI	Normalized Difference Turbidity Index
CMRI	Combined Mangrove Recognition Index
IM	Mangrove Damage Index
NDWI	Normalized Different Water Index
MCDM	Multi-Criteria Decision-Making
AHP	Analytical Hierarchy Process
FVI	Flood Vulnerability Index
CI	Consistency Index
CR	Consistency Ratio
RI	Random Index
GIS	Geographic Information System
WOA	Weighted Overlay Analysis
SD	Standard Deviation
DW Statistic	Durbin–Watson Statistic

ANOVA	Analysis of Variance
ZPR Value	Standardized Predicted Value
df	Degrees of Freedom
RMSE	Root Mean Square Error
ROC	Receiver Operating Characteristic
AUC	Area under the ROC Curve
IMD	India Meteorological Department
ESCS	Extremely Severe Cyclonic Strom
sig.	Significant
Std. Error	Standard Error
VIF	Variance Inflation Factor
LULC	Land Use Land Cover

Appendix A

$$CMRI = (NDVI - DWI) \tag{A1}$$

where

NDVI is the Normalized Difference Vegetation Index,

$$NDWI = (Green - NIR)/(Green + NIR) \tag{A2}$$

where

NIR is Near Infrared.

$$IM = (NIR - SWIR/NIR \times SWIR) \times 10{,}000 \tag{A3}$$

where

NIR is Near Infrared, and *SWIR* is Shortwave Infrared.

$$NDFI_2{}^{*} = (Red - SWIR)/(Red + SWIR) \tag{A4}$$

and

$$NDFI_3{}^{**} = (Blue - SWIR2)/(Blue + SWIR2) \tag{A5}$$

where

SWIR is Shortwave Infrared.

* This formula has been used for the construction of the NDFI map of 2010.

** This formula has been used for the construction of the NDFI map for 2021 and 2022.

$$A = \begin{bmatrix} a_{11} & a_{12} & \dots & \dots & a_{1n} \\ a_{21} & a_{22} & \dots & \dots & a_{2n} \\ \vdots & \vdots & \dots & \dots & \vdots \\ \vdots & \vdots & \dots & \dots & \vdots \\ a_{n1} & a_{n2} & \dots & \dots & a_{nn} \end{bmatrix} \tag{A6}$$

where A is the evaluation matrix, a_{ii} is equal to 1, a_{ij} is equal to $\frac{1}{a_{ji}}$, and n is the criteria for pairwise comparison.

$$a_{ij} = \frac{a_{ij}}{\sum_{j=1}^{n} a_{ij}} \tag{A7}$$

$$w_1 = \frac{\sum_{j=1}^{n} a_{ij}}{n} \tag{A8}$$

where *I*, *j* = *1,2,3*, . . ., *n*. *n* is the number of elements.

$$CI = \frac{\lambda_{max} - n}{n - 1} \tag{A9}$$

where *CI* (consistency index) is the degree of consistency, *n* is the number of matrix elements being compared, and *λmax* denotes the largest or major eigenvalue of the matrix.

$$CR = \frac{CI}{RI} \tag{A10}$$

where *CR* = consistency ratio, *CI* = consistency index, and *RI* = random index.

$$Weighted\ Overlay = \sum(Xi \times Wi) \tag{A11}$$

where

Xi is the cell value of the raster, and *Wi* is the corresponding weight.

$$Y = \beta_0 + \beta_1 X_1 + \ldots + \beta_n X_n + e_t \tag{A12}$$

where *Y* is the dependent variable (here, normalized difference flood index (NDFI)), X_1 is the independent variable, β_1 is a parameter, and e_t is the error. The data were collected from each administrative unit (there is a total of 19 C.D. blocks in the Indian Sundarbans) to obtain the correlation coefficient value.

$$F = \frac{Explained\ variance}{Unexplained\ variance} \tag{A13}$$

or,

$$F = \frac{Between - group\ variability}{Within - group\ variability} \tag{A14}$$

$$\sum_{i=1}^{k} ni(\overline{Y}i - \overline{Y})2/(K-1) \tag{A15}$$

where $\overline{Y}i$ denotes the sample mean in the *i*th group, *ni* is the number of observations in the *i*th group, $\overline{Y}$ denotes the overall mean of the data, and *K* denotes the number of groups.

$$\sum_{i=1}^{n}\sum_{j=1}^{ni} (Yij - \overline{Y}i.)2/(N-K) \tag{A16}$$

where *Yij* is the observation in the *i*th out of *K* groups, and *N* is the overall sample size.

$$RMSE = \sqrt{\frac{\sum_{i=1}^{n} (\hat{y}_i - y_i)^2}{n}} \tag{A17}$$

where

$\hat{y}_1, \hat{y}_2, \ldots, \hat{y}_n$ are predicted values;

$y_1, y_2, \ldots, y_n$ are observed values;

N is the number of observations.

$$t' = \frac{\overline{x}_1 - \overline{x}_2}{\sqrt{\frac{s_1^2}{n_1} + \frac{s_2^2}{n_2}}} \tag{A18}$$

where t' is the *t*-statistic.

Population means in this study are $\overline{x}_1$ and $\overline{x}_2$, while population variances are s_1 and s_2. Additionally, n_1 and n_2, respectively, represent the sums of the statistical populations 1 and 2.

Appendix B

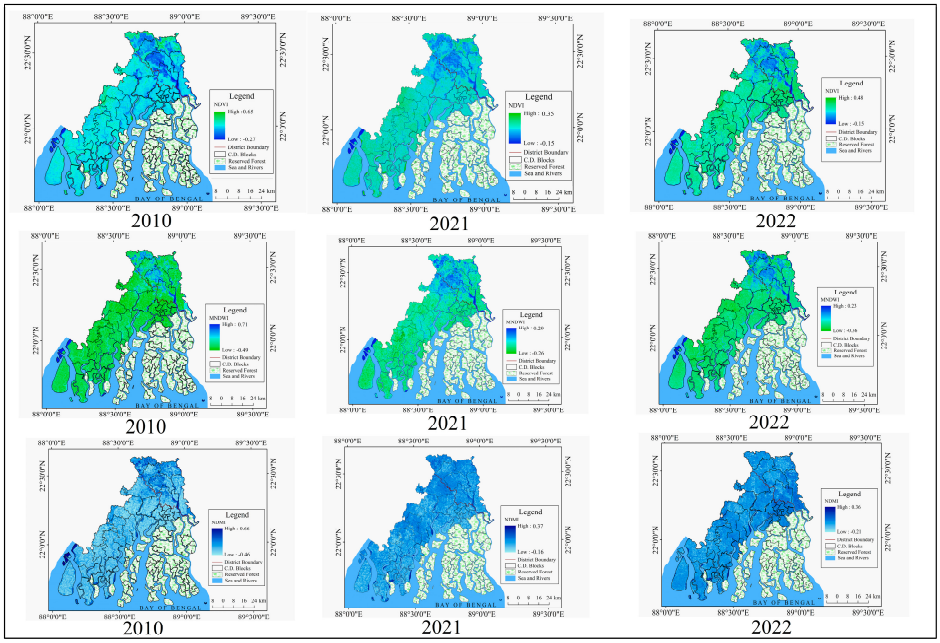


Figure A1. Conditions of NDVI, MNDWI, and NDMI in the Sundarbans (2010, 2021, and 2022).

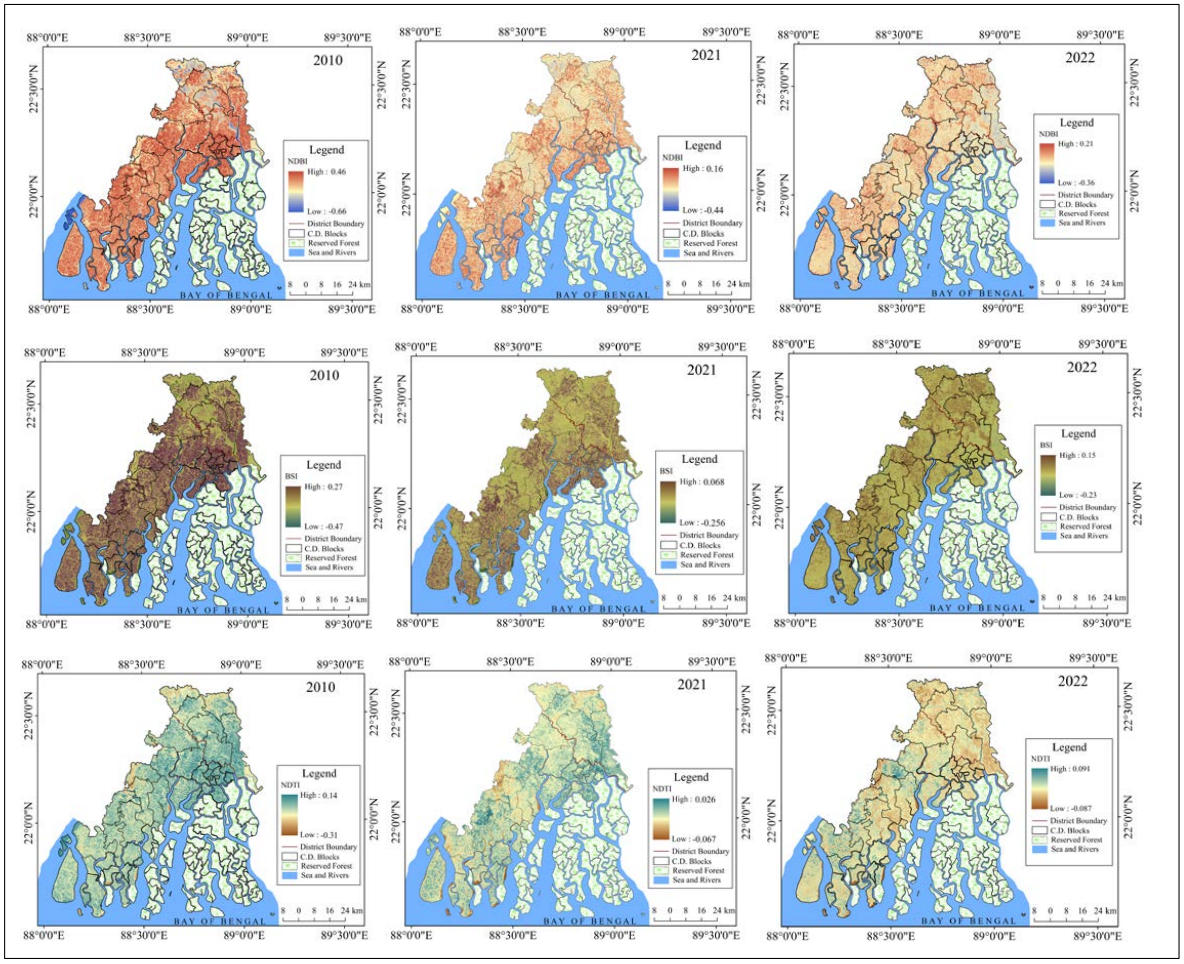


Figure A2. Conditions of NDBI, BSI, and NDTI in the Sundarbans (2010, 2021, and 2022).

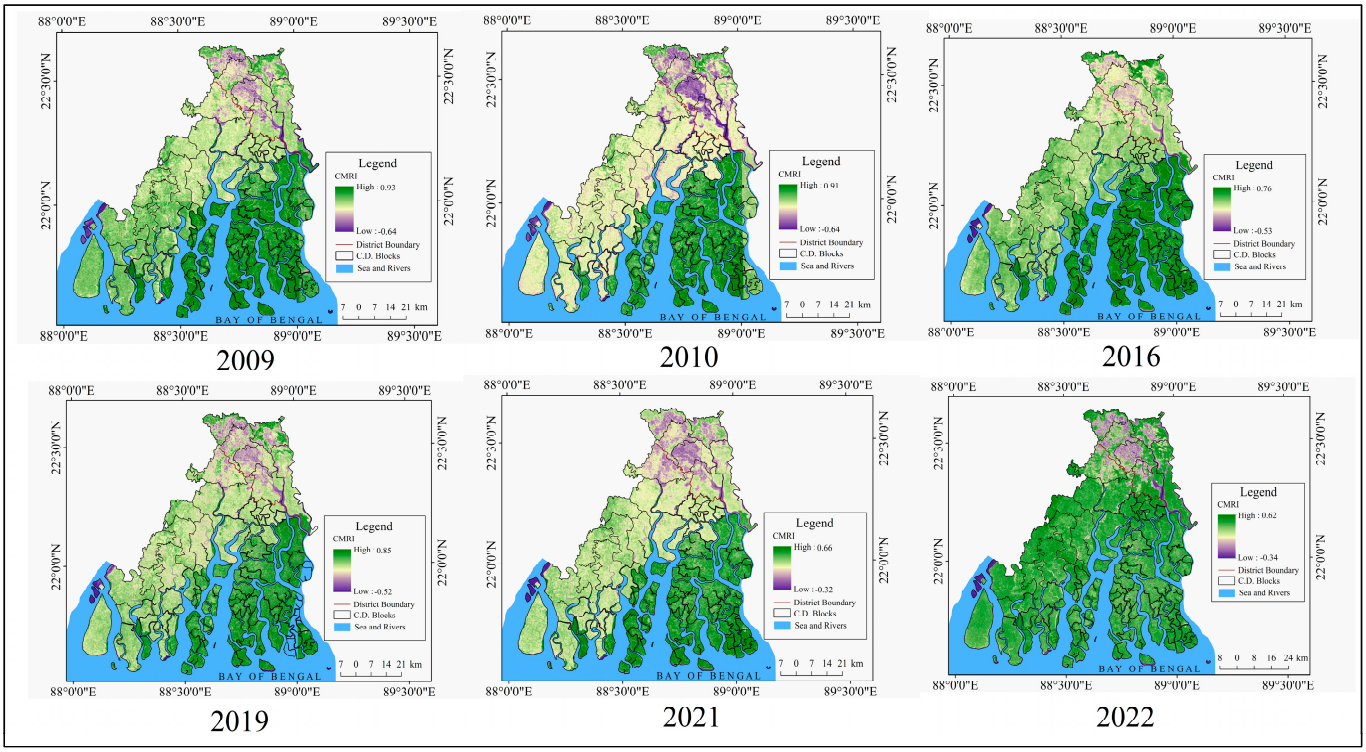


Figure A3. Combined Mangrove Recognition Index (CMRI) of the Sundarbans (2009, 2010, 2016, 2019, 2021, and 2022).

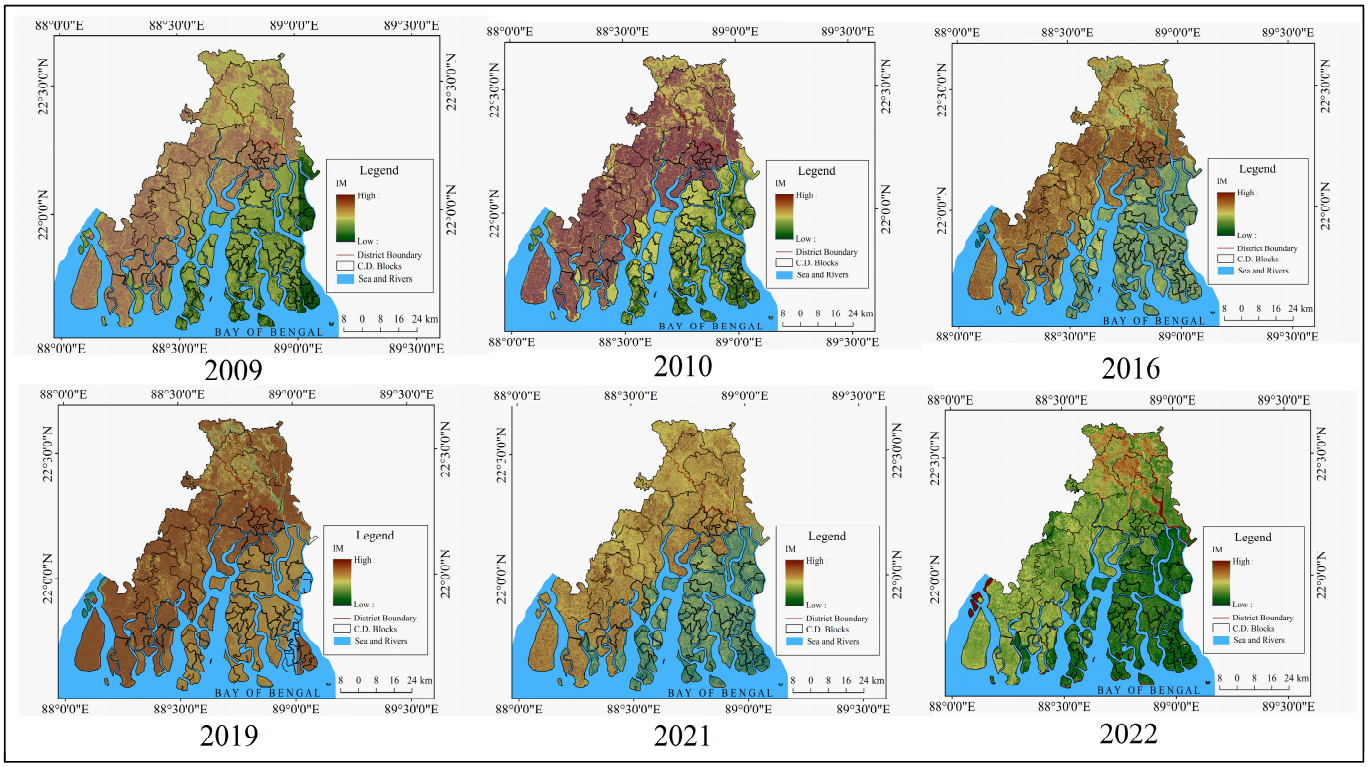


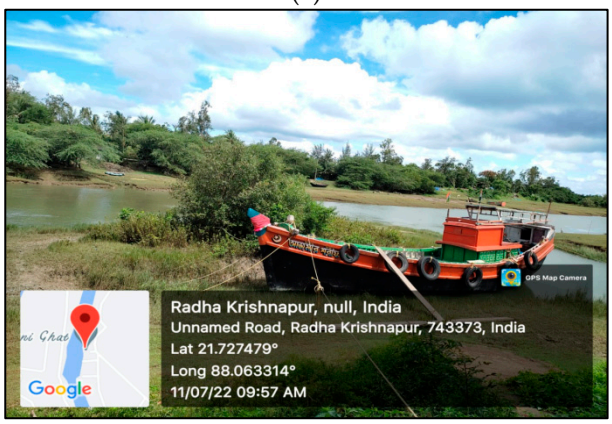
Figure A4. Mangrove damage conditions (IM) in the Sundarbans (2009, 2010, 2016, 2019, 2021, and 2022).



(**a**)



(**b**)



(**c**)



(**d**)



(**e**)



(**f**)



(**g**)



(**h**)

Figure A5. *Cont*.

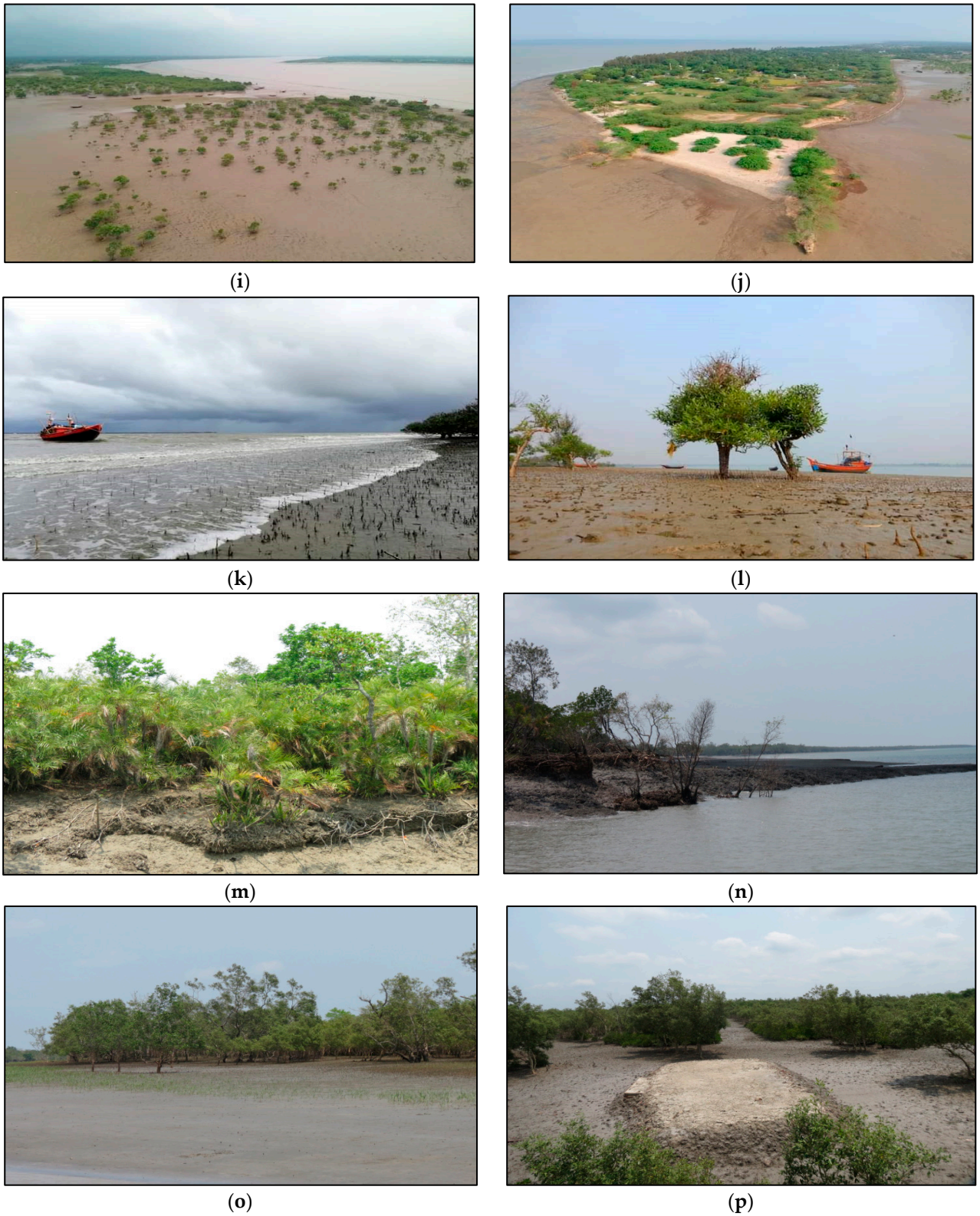


Figure A5. (**a**,**b**) Type of damage to Sagar's concrete roads and embankments near the beach in 2022. (**c**,**d**) A cyclone in Sagar in 2022 caused mangroves to creak and embankments to collapse. (**e**,**f**) Concrete and earthen embankment collapsed in Sagar in 2022 due to a cyclone. (**g**,**h**) Mangrove loss and damaged area on Mousuni Island, 2022. (**i**,**j**) Mangrove damage and deforestation on Mousuni Island, 2022. (**k**,**l**) The beach on Mousuni Island, 2022, with trees and mangrove seedlings. (**m**,**n**) Mangrove forest damage and beach debasement in Gosaba, 2019. (**o**,**p**) Cyclone damage to mangrove forest on Dobaki Island, Gosaba, 2019.

Appendix C

Table A1. Classification and reclassification of raster layers for weighted overlay analysis.

Years Spectral Indices	2010		2021		2022	
	Classified	**Reclassified**	**Classified**	**Reclassified**	**Classified**	**Reclassified**
NDVI	−0.27–−0.17	1	−0.14–−0.089	1	−0.15–−0.082	1
	−0.16–−0.072	2	−0.088–−0.034	2	−0.081–−0.012	2
	−0.071–0.027	3	−0.033–0.021	3	−0.011–0.059	3
	0.028–0.13	4	0.022–0.077	4	0.06–0.03	4
	0.14–0.23	5	0.078–0.13	5	0.14–0.20	5
	0.24–0.33	6	0.14–0.19	6	0.21–0.27	6
	0.34–0.43	7	0.2–0.24	7	0.28–0.34	7
	0.44–0.52	8	0.25–0.3	8	0.35–0.41	8
	0.53–0.62	9	0.31–0.35	9	0.42–0.48	9
MNDWI	−0.49–−0.35	1	−0.26–−0.2	1	−0.36–−0.30	1
	−0.34–−0.22	2	−0.19–−0.14	2	−0.29–−0.23	2
	−0.21–−0.09	3	−0.13–−0.074	3	−0.22–−0.16	3
	−0.089–0.043	4	−0.073–−0.012	4	−0.15–−0.10	4
	0.044–0.18	5	−0.011–0.05	5	−0.09–−0.034	5
	0.19–0.31	6	0.051–0.11	6	−0.033–0.031	6
	0.32–0.44	7	0.12–0.17	7	0.032–0.096	7
	0.45–0.57	8	0.18–0.24	8	0.097–0.16	8
	0.58–0.7	9	0.25–0.3	9	0.17–0.23	9
NDMI	−0.46–−0.34	1	−0.16–−0.097	1	−0.21–−0.14	1
	−0.33–−0.21	2	−0.096–−0.039	2	−0.13–−0.081	2
	−0.2–−0.087	3	−0.038–0.019	3	−0.08–−0.018	3
	−0.086–0.037	4	0.02–0.077	4	−0.017–0.044	4
	0.038–0.16	5	0.078–0.13	5	0.045–0.11	5
	0.17–0.29	6	0.14–0.19	6	0.12–0.17	6
	0.3–0.41	7	0.2–0.25	7	0.18–0.23	7
	0.42–0.54	8	0.26–0.31	8	0.24–0.29	8
	0.55–0.66	9	0.32–0.37	9	0.3–0.36	9
NDBI	−0.66–−0.54	1	−0.43–−0.37	1	−0.36–−0.29	1
	−0.53–−0.41	2	−0.36–−0.3	2	−0.28–−0.23	2
	−0.40–−0.29	3	−0.29–−0.24	3	−0.22–−0.17	3
	−0.28–−0.16	4	−0.23–−0.17	4	−0.16–−0.11	4
	−0.15–−0.037	5	−0.16–−0.11	5	−0.1–−0.044	5
	−0.036–0.087	6	−0.1–−0.042	6	−0.043–0.018	6
	0.088–0.21	7	−0.041–0.024	7	0.019–0.081	7
	0.22–0.34	8	0.025–0.09	8	0.082–0.14	8
	0.35–0.46	9	0.091–0.16	9	0.15–0.21	9
BSI	−0.47–−0.39	1	−0.26–−0.22	1	−0.23–−0.19	1
	−0.38–−0.31	2	−0.21–−0.18	2	−0.18–−0.15	2
	−0.30–−0.22	3	−0.17–−0.15	3	−0.14–−0.1	3
	−0.21–−0.14	4	−0.14–−0.11	4	−0.09–−0.062	4
	−0.13–−0.061	5	−0.1–−0.076	5	−0.061–−0.02	5
	−0.06–0.022	6	−0.075–−0.04	6	−0.019–0.022	6
	0.023–0.1	7	−0.039–−0.0039	7	0.023–0.063	7
	0.11–0.19	8	−0.0038–0.032	8	0.064–0.11	8
	0.20–0.27	9	0.033–0.068	9	0.12–0.15	9

Table A1. *Cont.*

Years Spectral Indices	2010		2021		2022	
	Classified	**Reclassified**	**Classified**	**Reclassified**	**Classified**	**Reclassified**
NDTI	−0.31–−0.26	1	−0.067–−0.056	1	−0.087–−0.067	1
	−0.25–−0.21	2	−0.055–−0.046	2	−0.066–−0.048	2
	−0.20–−0.16	3	−0.045–−0.036	3	−0.047–−0.028	3
	−0.15–−0.11	4	−0.035–−0.026	4	−0.027–−0.008	4
	−0.10–−0.057	5	−0.025–−0.015	5	−0.0079–0.012	5
	−0.056–−0.0068	6	−0.014–−0.005	6	0.013–0.032	6
	−0.0067–0.043	7	−0.0049–0.0053	7	0.033–0.051	7
	0.044–0.094	8	0.0054–0.016	8	0.052–0.071	8
	0.095–0.14	9	0.017–0.026	9	0.072–0.091	9

Table A2. Output of regression model (2022).

Model Summary [b]									
Model	R	R Square	Adjusted R Square	Std. Error of the Estimate	Durbin−Watson				
1	0.970 [a]	0.940	0.923	0.01493	1.914				
a. Predictors: (Constant), NDTI, NDVI, NDBI, BSI									
b. Dependent Variable: NDFI									
ANOVA [a]									
Model		Sum of Squares	df	Mean Square	F	Sig.			
1	Regression	0.049	4	0.012	55.045	0.000 [b]			
	Residual	0.003	14	0.000					
	Total	0.052	18						
a. Dependent Variable: NDFI									
b. Predictors: (Constant), NDTI, NDVI, NDBI, BSI									
Coefficients [a]									
Model		Unstandardized Coefficients		Standardized Coefficients	t	Sig. *	95.0% Confidence Interval for B		Collinearity Statistics	
		B	Std. Error	Beta			Lower Bound	Upper Bound	Tolerance	VIF
1	(Constant)	−0.031	0.033		−0.948	0.359	−0.103	0.040		
	NDVI	−0.658	0.093	−1.094	−7.047	0.000 **	−0.858	−0.458	0.177	5.644
	NDBI	−0.797	0.509	−0.809	−1.567	0.140	−1.889	0.294	0.016	62.488
	BSI	−0.168	0.924	−0.123	−0.182	0.858	−2.150	1.814	0.009	106.917
	NDTI	−0.709	0.598	−0.191	−1.186	0.255	−1.992	0.573	0.165	6.074
* The total number of observations (n) = 19 ** The p-value: Minimal but not quite zero										
a. Dependent Variable: NDFI										
Excluded Variables [a]										

Table A2. *Cont.*

Model		Beta In	t	Sig.	Partial Correlation	Collinearity Statistics		
						Tolerance	VIF	Minimum Tolerance
1	MNDWI	−10.801 [b]	−1.240	0.237	−0.325	0.000054220	18,443.399	0.0000370
	NDMI	.[b]	.	.	.	0.000 **	.	0.000 **
a. Dependent Variable: NDFI								
b. Predictors in the Model: (Constant), NDTI, NDVI, NDBI, BSI								

Table A3. Block-wise NDFI and standardized predicted values of flood susceptibility probability.

C.D. Blocks	NDFI (2010)	NDFI (2021)	NDFI (2022)	ZPR (2010)	ZPR (2021)	ZPR (2022)
Canning−I	−0.45946	0.095745	−0.1211	−0.78611	0.08813	−1.46359
Canning−II	−0.38235	0.193871	−0.06753	−0.38926	1.41659	−0.79838
Mathurapur−I	−0.36585	−0.03463	−0.11512	−1.13422	−1.75122	−0.64429
Jaynagar−I	−0.39	0.06398	−0.05454	0.00452	−0.37661	−0.88091
Jaynagar−II	−0.32489	0.102167	−0.07834	−0.20735	0.17996	−0.28575
Kultali	−0.17073	0.163889	−0.01618	0.79065	1.04404	1.06068
Basanti	−0.39932	0.138561	−0.0736	−0.39557	0.67979	−0.92696
Gosaba	−0.1746	0.141982	−0.00988	1.32131	0.75628	1.04259
Mathurapur−II	−0.1677	0.238038	0.037978	1.71383	2.07778	1.09658
Kakdwip	−0.43357	0.057409	−0.08345	−0.68745	−0.45934	−1.23924
Sagar	−0.37255	0.006768	−0.05907	−0.37587	−1.1838	−0.7058
Namkhana	−0.37165	0.098237	−0.05341	−0.23713	0.12614	−0.69482
Patharpratima	−0.39785	−0.00271	−0.07171	−0.54458	−1.2942	−0.91281
Haroa	−0.2	0.124469	0.093731	2.78633	0.52248	0.82285
Minakhan	−0.19313	−0.0265	−0.12439	−0.97659	−1.62789	0.86377
Sandeshkhali−I	−0.19588	0.084123	−0.08168	−0.62304	−0.09262	0.85849
Sandeshkhali−II	−0.07027	0.078758	−0.10111	−0.5549	−0.12813	1.94128
Hasnabad	−0.25604	0.07904	−0.04405	0.0683	−0.14953	0.33297
Hingalganj	−0.23077	0.102639	−0.06347	0.22712	0.17214	0.53333

References

1. Ostling, J.L.; Butler, D.R.; Dixon, R.W. The biogeomorphology of mangroves and their role in natural hazards mitigation. *Geogr. Compass* **2009**, *3*, 1607–1624. [CrossRef]
2. Karimi, Z.; Abdi, E.; Deljouei, A.; Cislaghi, A.; Shirvany, A.; Schwarz, M.; Hales, T.C. Vegetation-induced soil stabilization in coastal area: An example from a natural mangrove forest. *Catena* **2022**, *216*, 106410. [CrossRef]
3. Leal Filho, W.; Alam, G.M.; Nagy, G.J.; Rahman, M.M.; Roy, S.; Wolf, F.; Kovaleva, M.; Saroar, M.; Li, C. Climate change adaptation responses among riparian settlements: A case study from Bangladesh. *PLoS ONE* **2022**, *17*, e0278605. [CrossRef] [PubMed]
4. Mitra, A.; Dutta, J.; Mitra, A.; Thakur, T. Amphan Super cyclone: A death knell for Indian Sundarbans. *J. Appl. For. Ecol.* **2020**, *8*, 41–48.
5. Das, C.S.; Mallick, D.; Mandal, R.N. Mangrove Forests in Changing Climate: A Global Overview. *J. Indian Soc. Coast. Agric. Res.* **2020**, *38*, 104–124.
6. Siegert, M.; Alley, R.B.; Rignot, E.; Englander, J.; Corell, R. Twenty-first century sea-level rise could exceed IPCC projections for strong-warming futures. *One Earth* **2020**, *3*, 691–703. [CrossRef]
7. Sobhani, P.; Esmaeilzadeh, H.; Barghjelveh, S.; Sadeghi, S.M.; Marcu, M.V. Habitat integrity in protected areas threatened by LULC changes and fragmentation: A case study in Tehran province, Iran. *Land* **2021**, *11*, 6. [CrossRef]
8. Moradi, F.; Sadeghi, S.M.; Heidarlou, H.B.; Deljouei, A.; Boshkar, E.; Borz, S.A. Above-ground biomass estimation in a Mediterranean sparse coppice oak forest using Sentinel-2 data. *Ann. For. Res.* **2022**, *65*, 165–182. [CrossRef]
9. Pourreza, M.; Moradi, F.; Khosravi, M.; Deljouei, A.; Vanderhoof, M.K. GCPs-free photogrammetry for estimating tree height and crown diameter in Arizona Cypress plantation using UAV-mounted GNSS RTK. *Forests* **2022**, *13*, 1905. [CrossRef]
10. Sobhani, P.; Esmaeilzadeh, H.; Deljouei, A.; Wolf, I.D.; Marcu, M.V.; Sadeghi, S.M. Assessing water security and footprint in hypersaline Lake Urmia. *Ecol. Indic.* **2023**, *155*, 110955. [CrossRef]
11. Sakib, M. Sundarban as a buffer against storm surge flooding. *World J. Eng. Technol.* **2015**, *3*, 59. [CrossRef]
12. Gayathri, R.; Murty, P.L.; Bhaskaran, P.K.; Srinivasa; Kumar, T. A. Numerical study of hypothetical storm surge and coastal inundation for AILA cyclone in the Bay of Bengal. *Environ. Fluid Mech.* **2016**, *16*, 429–452. [CrossRef]

13. Rahman, S.; Rahman, H.; Shahid, S.; Khan, R.U.; Jahan, N.; Ahmed, Z.U.; Khanum, R.; Ahmed, M.F.; Mohsenipour, M. The impact of cyclone Aila on the Sundarban forest ecosystem. *Int. J. Ecol. Dev.* **2017**, *32*, 87–97.
14. Sharma, S.; Suwa, R.; Ray, R.; Mandal, M.S. Successive cyclones attacked the world's largest mangrove forest located in the Bay of Bengal under pandemic. *Sustainability* **2022**, *14*, 5130. [CrossRef]
15. Mondal, P.; Dutta, T.; Qadir, A.; Sharma, S. Radar and optical remote sensing for near real-time assessments of cyclone impacts on coastal ecosystems. *Remote Sens. Ecol.* **2022**, *8*, 506–520. [CrossRef] [PubMed]
16. Deb, M.; Ferreira, C.M. Potential impacts of the Sunderban mangrove degradation on future coastal flooding in Bangladesh. *J. Hydro-Environ. Res.* **2017**, *17*, 30–46. [CrossRef]
17. Bahinipati, C.S.; Sahu, N. Mangrove conservation as a sustainable adaptation to cyclonic risk in Kendrapada District of Odisha, India. *Asian J. Environ. Disaster Manag.* **2012**, *4*, 183–202. [CrossRef]
18. Ghosh, A.; Schmidt, S.; Fickert, T.; Nüsser, M. The Indian Sundarban mangrove forests: History, utilization, conservation strategies and local perception. *Diversity* **2015**, *7*, 149–169. [CrossRef]
19. Samanta, S.; Hazra, S.; Mondal, P.P.; Chanda, A.; Giri, S.; French, J.R.; Nicholls, R.J. Assessment and attribution of mangrove Forest changes in the Indian Sundarbans from 2000 to 2020. *Remote Sens.* **2021**, *13*, 4957. [CrossRef]
20. Giri, C.; Pengra, B.; Zhu, Z.; Singh, A.; Tieszen, L.L. Monitoring mangrove forest dynamics of the Sundarbans in Bangladesh and India using multi-temporal satellite data from 1973 to 2000. *Estuar. Coast. Shelf Sci.* **2007**, *73*, 91–100. [CrossRef]
21. Kumar, D.; Bhattacharjya, R.K. Review of different methods and techniques used for flood vulnerability analysis. *Nat. Hazards Earth Syst. Sci.* **2020**, 11–30.
22. Ali, M.; Tasnim Mukarram, M.; Islam, A. Environmental Degradation Due to Deforestation in the Sundarban Forest of Bangladesh. *Int. J. Sci. Eng. Res.* **2021**, *12*, 855–862.
23. Majumder, R.; Ghosh, D.K.; Mandal, A.C.; Patra, P.; Bhunia, G.S. An appraisal of geomorphic characteristics and flood susceptibility zone using remote sensing and GIS: A case study in Bongaon Subdivision, North 24 Parganas (West Bengal), India. *Int. J. Res. Geogr.* **2017**, *3*, 32–40.
24. Sahana, M.; Rehman, S.; Sajjad, H.; Hong, H. Exploring effectiveness of frequency ratio and support vector machine models in storm surge flood susceptibility assessment: A study of Sundarban Biosphere Reserve, India. *Catena* **2020**, *189*, 104450. [CrossRef]
25. Sahana, M.; Sajjad, H. Vulnerability to storm surge flood using remote sensing and GIS techniques: A study on Sundarban Biosphere Reserve, India. *Remote Sens. Appl. Soc. Environ.* **2019**, *13*, 106–120. [CrossRef]
26. Jana, R.; Mohapatra, S.; Gupta, A. Vulnerability to cyclone disaster in Indian Sundarbans: A micro-level analysis. *Hill Geographer.* **2017**, *XXXIII*, 1–15.
27. Bera, A.; Meraj, G.; Kanga, S.; Farooq, M.; Singh, S.K.; Sahu, N.; Kumar, P. Vulnerability and risk assessment to climate change in Sagar Island, India. *Water* **2022**, *14*, 823. [CrossRef]
28. Sahana, M.; Hong, H.; Ahmed, R.; Patel, P.P.; Bhakat, P.; Sajjad, H. Assessing coastal island vulnerability in the Sundarban Biosphere Reserve, India, using geospatial technology. *Environ. Earth Sci.* **2019**, *78*, 1–22. [CrossRef]
29. Ali, S.A.; Khatun, R.; Ahmad, A.; Ahmad, S.N. Assessment of cyclone vulnerability, hazard evaluation and mitigation capacity for analyzing cyclone risk using GIS technique: A study on Sundarban biosphere reserve, India. *Earth Syst. Environ.* **2020**, *4*, 71–92. [CrossRef]
30. Mondal, B.K. Nature of propensity of Indian Sundarban. *Int. J. Appl. Res.* **2015**, *4*, 1–17.
31. Mondal, B.K. Assessment of effects of global warming and climate change on the vulnerability of Indian Sundarban. In *Sustainable Development: Dynamic Perspective*; Anjan Publisher: Kolkata, India, 2018; pp. 63–74.
32. Mondal, B.K. Climate change induced coastal hazards and community vulnerability in Indian Sundarban. In *Applied Geomorphology and Contemporary Issues*; Springer International Publishing: Cham, Switzerland, 2022; pp. 587–609.
33. USGS (United States Geological Survey). *Landsat Data Access*; Department of Interior, United States Geological Survey: Washington, DC, USA, 2021. Available online: https://earthexplorer.usgs.gov/ (accessed on 26 December 2022).
34. USGS (United States Geological Survey). *Landsat Data Access*; Department of Interior, United States Geological Survey: Washington, DC, USA, 2022. Available online: https://earthexplorer.usgs.gov/ (accessed on 26 December 2022).
35. NRSC (National Remote Sensing Centre). *Resourcesat-1/Resoursat-2: LISS-III*; Government of India: New Delhi, India, 2009. Available online: https://bhuvan.nrsc.gov.in/home/index.php (accessed on 23 December 2022).
36. NRSC (National Remote Sensing Centre). *Resourcesat-1/Resoursat-2: AWiFS*; Government of India: New Delhi, India, 2010. Available online: https://bhuvan.nrsc.gov.in/home/index.php (accessed on 22 December 2022).
37. NRSC (National Remote Sensing Centre). *Resourcesat-1/Resoursat-2: LISS-III*; Government of India: New Delhi, India, 2016. Available online: https://bhuvan.nrsc.gov.in/home/index.php (accessed on 3 January 2023).
38. NRSC (National Remote Sensing Centre). *Resourcesat-1/Resoursat-2: LISS-III*; Government of India: New Delhi, India, 2019. Available online: https://bhuvan.nrsc.gov.in/home/index.php (accessed on 26 December 2022).
39. India Meteorological Department. *Climatological Table*; Ministry of Earth Sciences, Government of India: New Delhi, India, 2010.
40. India Meteorological Department. *Climatological Table*; Ministry of Earth Sciences, Government of India: New Delhi, India, 2021.
41. India Meteorological Department. *Climatological Table*; Ministry of Earth Sciences, Government of India: New Delhi, India, 2022.
42. Global Modeling and Assimilation Office (GMAO). *MERRA-2 Day and Month-wise Rainfall Data of Selected Coordinate Points in West Bengal, India*; Goddard Earth Sciences Data and Information Services Center (GES DISC): Greenbelt, MD, USA, 2010.

43. Global Modeling and Assimilation Office (GMAO). *MERRA-2 Day and Month-Wise Rainfall Data of Selected Coordinate Points in West Bengal, India*; Goddard Earth Sciences Data and Information Services Center (GES DISC): Greenbelt, MD, USA, 2021.
44. Global Modeling and Assimilation Office (GMAO). *MERRA-2 Day and Month-Wise Rainfall Data of Selected Coordinate Points in West Bengal, India*; Goddard Earth Sciences Data and Information Services Center (GES DISC): Greenbelt, MD, USA, 2022.
45. Rouse, J.W., Jr.; Haas, R.H.; Schell, J.A.; Deering, D.W. Monitoring Vegetation Systems in the Great Plains with ERTS. In *Proceedings of the Third Earth Resources Technology Satellite-1 Symposium: Section AB, Technical presentations, Greenbelt, MY, USA, 10—14 December 1973*; Scientific and Technical Information Office: Oak Ridge, TN, USA; National Aeronautics and Space Administration: Washington, DC, USA, 1974; Volume 1, Paper a 20; pp. 309–317.
46. Xu, H. A study on information extraction of water body with the modified normalized difference water index (MNDWI). *J. Remote Sens.-Beijing* **2005**, *9*, 589–595.
47. Gao, B.C. NDWI—A normalized difference water index for remote sensing of vegetation liquid water from space. *Remote Sens. Environ.* **1996**, *58*, 257–266. [CrossRef]
48. Diek, S.; Fornallaz, F.; Schaepman, M.E.; De Jong, R. Barest pixel composite for agricultural areas using landsat time series. *Remote Sens.* **2017**, *9*, 1245. [CrossRef]
49. Rikimaru, A.; Roy, P.S.; Miyatake, S. Tropical Forest cover density mapping. *Trop. Ecol.* **2002**, *43*, 39–47.
50. Piyoosh, A.K.; Ghosh, S.K. Development of a modified bare soil and urban index for Landsat 8 satellite data. *Geocarto Int.* **2018**, *33*, 423–442. [CrossRef]
51. Zha, Y.; Gao, J.; Ni, S. Use of normalized difference built-up index in automatically mapping urban areas from TM imagery. *Int. J. Remote Sens.* **2003**, *24*, 583–594. [CrossRef]
52. Elhag, M.; Gitas, I.; Othman, A.; Bahrawi, J.; Gikas, P. Assessment of water quality parameters using temporal remote sensing spectral reflectance in arid environments, Saudi Arabia. *Water* **2019**, *11*, 556. [CrossRef]
53. Lacaux, J.P.; Tourre, Y.M.; Vignolles, C.; Ndione, J.A.; Lafaye, M. Classification of ponds from high-spatial resolution remote sensing: Application to Rift Valley Fever epidemics in Senegal. *Remote Sens. Environ.* **2007**, *106*, 66–74. [CrossRef]
54. Gupta, K.; Mukhopadhyay, A.; Giri, S.; Chanda, A.; Majumdar, S.D.; Samanta, S.; Mitra, D.; Samal, R.N.; Pattnaik, A.K.; Hazra, S. An index for discrimination of mangroves from non-mangroves using LANDSAT 8 OLI imagery. *MethodsX* **2018**, *5*, 1129–1139. [CrossRef] [PubMed]
55. McFeeters, S.K. The use of the Normalized Difference Water Index (NDWI) in the delineation of open water features. *Int. J. Remote Sens.* **1996**, *17*, 1425–1432. [CrossRef]
56. Winarso, G.; Purwanto, A.D. Evaluation of mangrove damage level based on Landsat 8 image. *Int. J. Remote Sens. Earth Sci.* **2014**, *11*, 105–116. [CrossRef]
57. Boschetti, M.; Nutini, F.; Manfron, G.; Brivio, P.A.; Nelson, A. Comparative analysis of normalised difference spectral indices derived from MODIS for detecting surface water in flooded rice cropping systems. *PLoS ONE* **2014**, *9*, e88741. [CrossRef] [PubMed]
58. Wan, K.M.; Billa, L. Post-flood land use damage estimation using improved Normalized Difference Flood Index (NDFI3) on Landsat 8 datasets: December 2014 floods, Kelantan, Malaysia. *Arab. J. Geosci.* **2018**, *11*, 434. [CrossRef]
59. Ali, S.A.; Khatun, R.; Ahmad, A.; Ahmad, S.N. Application of GIS-based analytic hierarchy process and frequency ratio model to flood vulnerable mapping and risk area estimation at Sundarban region, India. *Model. Earth Syst. Environ.* **2019**, *5*, 1083–1102. [CrossRef]
60. Bera, R.; Maiti, R. Multi hazards risk assessment of Indian Sundarbans using GIS based Analytic Hierarchy Process (AHP). *Reg. Stud. Mar. Sci.* **2021**, *44*, 101766. [CrossRef]
61. Arif, M.S.; Mahdi, I.; Rafi, M.A.; Khan, S.J.; Rahman, M.M. Cyclone exposure mapping in coastal Bangladesh: A multi-criteria decision analysis. *Heliyon* **2023**, *9*, e21259. [CrossRef] [PubMed]
62. Ghosh, A.; Chatterjee, U.; Pal, S.C.; Towfiqul Islam, A.R.; Alam, E.; Islam, M.K. Flood hazard mapping using GIS-based statistical model in vulnerable riparian regions of sub-tropical environment. *Geocarto Int.* **2023**, *38*, 2285355. [CrossRef]
63. Kaya, C.M.; Derin, L. Parameters and methods used in flood susceptibility mapping: A review. *J. Water Clim. Chang.* **2023**, *14*, 1935–1960. [CrossRef]
64. Mohanty, S.; Mustak, S.; Singh, D.; Van Hoang, T.; Mondal, M.; Wang, C.T. Vulnerability and risk assessment mapping of Bhitarkanika national park, Odisha, India using machine-based embedded decision support system. *Front. Environ. Sci.* **2023**, *11*, 1176547. [CrossRef]
65. Saaty, R.W. The analytic hierarchy process—What it is and how it is used. *Math. Model.* **1987**, *9*, 161–176. [CrossRef]
66. Bozdağ, A.; Yavuz, F.; Günay, A.S. AHP and GIS based land suitability analysis for Cihanbeyli (Turkey) County. *Environ. Earth Sci.* **2016**, *75*, 813. [CrossRef]
67. Saaty, T.L. A scaling method for priorities in hierarchical structures. *J. Math. Psychol.* **1977**, *15*, 234–281. [CrossRef]
68. Saaty, T.L. *The Analytic Hierarchy Process*; Mcgraw Hill: New York, NY, USA, 1980.
69. Abu Dabous, S.; Alkass, S. Decision support method for multi-criteria selection of bridge rehabilitation strategy. *Constr. Manag. Econ.* **2008**, *26*, 883–893. [CrossRef]
70. Bhushan, N.; Rai, K. The analytic hierarchy process. In *Strategic Decision Making: Applying the Analytic Hierarchy Process*; Springer: London, UK, 2004; pp. 11–21.

71. Shankar, S.V.; Dharanirajan, K.; Narshimulu, G. Cyclone vulnerability zonation of southern part of South Andaman, India using Multi-criteria weighted overlay analysis techniques. *Indian J. Geo-Mar. Sci.* **2015**, *44*, 1181–1190.
72. Nikolova, V.; Zlateva, P. Assessment of flood vulnerability using fuzzy logic and geographical information systems. In *Information Technology in Disaster Risk Reduction: First IFIP TC 5 DCITDRR International Conference, ITDRR 2016, Sofia, Bulgaria, 16–18 November 2016*; Revised Selected Papers 1; Springer International Publishing: Berlin/Heidelberg, Germany, 2017; pp. 254–265.
73. Batbold, B.; Bolorchuluun, C. Flood Risk Mapping Using GIS-Based Multi-Criteria Analysis: Songinokhairkhan District Case Study. In *Proceedings of the Climate Risks and Space Weather, Glasgow, Scotland, 14–17 June 2021*; Irkutsk State University: Irkutsk, Russia, 2021; pp. 67–76.
74. Hossain, M.Z.; Adhikary, S.K. Flood Susceptibility Assessment in Southwest Coastal Region of Bangladesh Using an AHP-GIS Based Approach. In Proceedings of the 6th International Conference on Advances in Civil Engineering (ICACE-2022), CUET, Chattogram, Bangladesh, 21–23 December 2022; 2024; pp. 1129–1136. Available online: www.cuet.ac.bd/icace (accessed on 12 January 2024).
75. Santosa, B.H.; Martono, D.N.; Purwanaa, R.; Koestoera, R.H. Flood Vulnerability Evaluation and Prediction Using Multi-temporal Data: A Case in Tangerang, Indonesia. *Int. J. Adv. Sci. Eng. Inf. Technol.* **2022**, *12*, 2156–2164. [CrossRef]
76. AlAli, A.M.; Salih, A.; Hassaballa, A. Geospatial-Based Analytical Hierarchy Process (AHP) and Weighted Product Model (WPM) Techniques for Mapping and Assessing Flood Susceptibility in the Wadi Hanifah Drainage Basin, Riyadh Region, Saudi Arabia. *Water* **2023**, *15*, 1943. [CrossRef]
77. Wijesinghe, W.M.; Mishra, P.K.; Tripathi, S.; Abdelrahman, K.; Tiwari, A.; Fnais, M.S. Integrated Flood Hazard Vulnerability Modeling of Neluwa (Sri Lanka) Using Analytical Hierarchy Process and Geospatial Techniques. *Water* **2023**, *15*, 1212. [CrossRef]
78. Durbin, J.; Watson, G.S. Testing For Serial Correlation in Least Squares Regression. III. *Biometrika* **1971**, *58*, 1–19. [CrossRef]
79. Fisher, R.A. Statistical Methods for Research Workers. In *Nature*, 6th ed.; Oliver and Boyd: London, UK, 1936; p. xiv+339.
80. Uyanik, G.; Guler, N. A study on multiple linear regression. *Procedia Soc. Behav. Sci.* **2013**, *106*, 234–240. [CrossRef]
81. Chai, T.; Draxler, R.R. Root mean square error (RMSE) or mean absolute error (MAE)?–Arguments against avoiding RMSE in the literature. *Geosci. Model Dev.* **2014**, *7*, 1247–1250. [CrossRef]
82. Welch, B.L. The generalization of 'student's' problem when several different population variances are involved. *Biometrika* **1947**, *34*, 28–35. [CrossRef] [PubMed]
83. Kanani-Sadat, Y.; Arabsheibani, R.; Karimipour, F.; Nasseri, M. A new approach to flood susceptibility assessment in data-scarce and ungauged regions based on GIS-based hybrid multi criteria decision-making method. *J. Hydrol.* **2019**, *572*, 17–31. [CrossRef]
84. Roopnarine, C.; Ramlal, B.; Roopnarine, R. A Comparative Analysis of Weighting Methods in Geospatial Flood Risk Assessment: A Trinidad Case Study. *Land* **2022**, *11*, 1649. [CrossRef]
85. India Meteorological Department. *Cyclonic Disturbances over North Indian Ocean during 2009: A Report*; Cyclone Warning Division: New Delhi, India, 2010.
86. India Meteorological Department. *Cyclonic Storm, KOMEN over the Bay of Bengal (26 July–02 August, 2015): A Report*; Earth System Science Organisation, Ministry of Earth Sciences, Government of India: New Delhi, India, 2015.
87. India Meteorological Department. *Extremely Severe Cyclonic Storm "FANI" over Eastcentral Equatorial Indian Ocean and Adjoining Southeast Bay of Bengal*; Regional Specialised Meteorological Centre-Tropical Cyclones: New Delhi, India, 2019.
88. India Meteorological Department. *Bulletin No.: 26 (Bay of Bengal 01/2020) Cyclone Warning Division*; Earth System Science Organisation (Ministry of Earth Sciences), Government of India: New Delhi, India, 2020.
89. India Meteorological Department. *Bulletin No.: 20 (BOB/02/2021)*; Ministry of Earth Sciences, Government of India: New Delhi, India, 2021.
90. Pearson, K. Mathematical contributions to the theory of evolution—On a form of spurious correlation which may arise when indices are used in the measurement of organs. *Proc. R. Soc. Lond.* **1897**, *60*, 489–498.
91. Pearson, K. On certain errors with regard to multiple correlation occasionally made by those who have not adequately studied this subject. *Biometrika* **1914**, *10*, 181–187.
92. Datta, D.; Deb, S. Analysis of coastal land use/land cover changes in the Indian Sunderbans using remotely sensed data. *Geo-Spat. Inf. Sci.* **2012**, *15*, 241–250. [CrossRef]
93. Hossain, K.A.; Masiero, M.; Pirotti, F. Land cover change across 45 years in the world's largest mangrove forest (Sundarbans): The contribution of remote sensing in forest monitoring. *Eur. J. Remote Sens.* **2022**, *12*, 1–7. [CrossRef]
94. Bera, M.K. Collective efforts of people to reduce disasters in the Indian Sundarban islands. *Disaster Prev. Manag.* **2019**, *28*, 691–705. [CrossRef]
95. Mondal, M.; Biswas, A.; Haldar, S.; Mandal, S.; Mandal, P.; Bhattacharya, S.; Paul, S. Climate change, multi-hazards and society: An empirical study on the coastal community of Indian Sundarban. *Nat. Hazards Res.* **2022**, *2*, 84–96. [CrossRef]
96. Sudha Rani, N.N.; Satyanarayana, A.N.; Bhaskaran, P.K. Coastal vulnerability assessment studies over India: A review. *Nat. Hazards* **2015**, *77*, 405–428. [CrossRef]

Disclaimer/Publisher's Note: The statements, opinions and data contained in all publications are solely those of the individual author(s) and contributor(s) and not of MDPI and/or the editor(s). MDPI and/or the editor(s) disclaim responsibility for any injury to people or property resulting from any ideas, methods, instructions or products referred to in the content.